Article

Cell

Single-Molecule Studies of Origin Licensing Reveal Mechanisms Ensuring Bidirectional Helicase Loading

Graphical Abstract

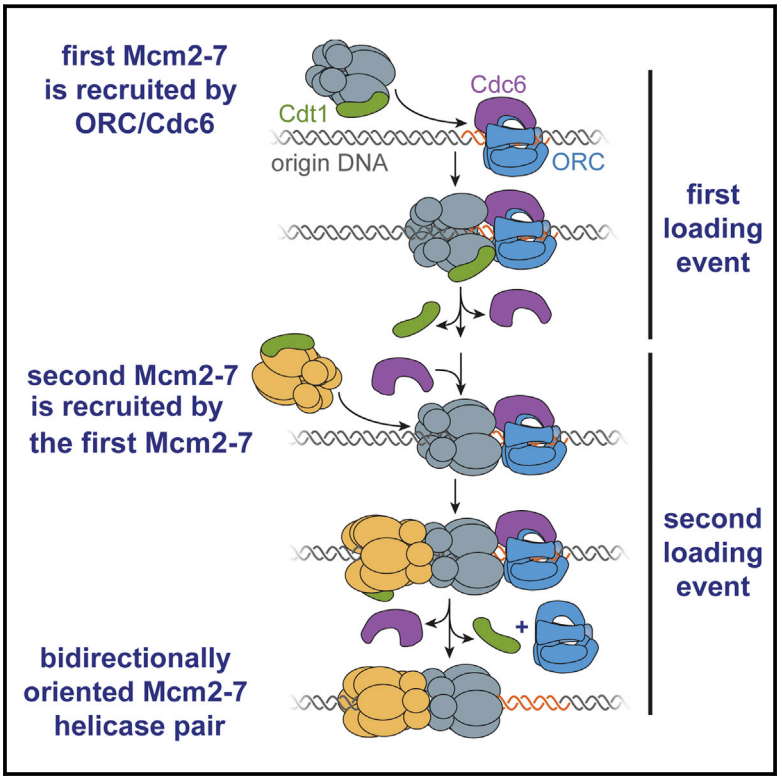

Highlights

- Single-molecule studies of origin licensing reveal new steps in helicase loading
- Two rounds of ordered Cdc6 and Cdt1 DNA binding and release direct helicase loading
- One ORC protein sequentially loads two Mcm2–7 to form a head-to-head double hexamer
- Distinct mechanisms load the two Mcm2–7 complexes, ensuring bidirectional assembly

Authors

Simina Ticau, Larry J. Friedman, ..., Jeff Gelles, Stephen P. Bell

Correspondence

gelles@brandeis.edu (J.G.), spbell@mit.edu (S.P.B.)

In Brief

Single-molecule assays reveal that loading of the two replicative helicase complexes at eukaryotic origins depends on two distinct mechanisms and that helicase-helicase interactions ensure their proper orientation to initiate bidirectional replisome assembly.

Ticau et al., 2015, Cell *161*, 513–525
April 23, 2015
http://dx.doi.org/10.1016/j.cell.2015.03.012

CellPress

Article

Cell

Single-Molecule Studies of Origin Licensing Reveal Mechanisms Ensuring Bidirectional Helicase Loading

Simina Ticau,[1] Larry J. Friedman,[2] Nikola A. Ivica,[1] Jeff Gelles,[2,*] and Stephen P. Bell[1,*]
[1]Howard Hughes Medical Institute, Department of Biology, Massachusetts Institute of Technology, Cambridge, MA 02139, USA
[2]Department of Biochemistry, Brandeis University, Waltham, MA 02454, USA
*Correspondence: gelles@brandeis.edu (J.G.), spbell@mit.edu (S.P.B.)
http://dx.doi.org/10.1016/j.cell.2015.03.012

SUMMARY

Loading of the ring-shaped Mcm2–7 replicative helicase around DNA licenses eukaryotic origins of replication. During loading, Cdc6, Cdt1, and the origin-recognition complex (ORC) assemble two heterohexameric Mcm2–7 complexes into a head-to-head double hexamer that facilitates bidirectional replication initiation. Using multi-wavelength single-molecule fluorescence to monitor the events of helicase loading, we demonstrate that double-hexamer formation is the result of sequential loading of individual Mcm2–7 complexes. Loading of each Mcm2–7 molecule involves the ordered association and dissociation of distinct Cdc6 and Cdt1 proteins. In contrast, one ORC molecule directs loading of both helicases in each double hexamer. Based on single-molecule FRET, arrival of the second Mcm2–7 results in rapid double-hexamer formation that anticipates Cdc6 and Cdt1 release, suggesting that Mcm-Mcm interactions recruit the second helicase. Our findings reveal the complex protein dynamics that coordinate helicase loading and indicate that distinct mechanisms load the oppositely oriented helicases that are central to bidirectional replication initiation.

INTRODUCTION

Eukaryotic DNA replication must occur faithfully each cell cycle to maintain genomic stability. Initiation of replication occurs at genomic sites called origins. To ensure that no origin initiates replication more than once per cell cycle, the cell restricts the DNA loading and activation of the Mcm2–7 replicative helicase to distinct cell-cycle stages (Siddiqui et al., 2013). Importantly, helicase loading (also known as pre-RC formation) licenses origins of replication by establishing the correct architecture for helicase activation and bidirectional replication initiation.

Three helicase-loading proteins direct Mcm2–7 loading: the origin recognition complex (ORC), Cdc6, and Cdt1 (reviewed in Yardimci and Walter, 2014). ORC binds origins of replication and recruits Cdc6 at the M/G1 transition. Cdc6-bound ORC recruits Mcm2–7 in complex with Cdt1 to origin DNA. In an ATP-hydrolysis-dependent reaction, recruited Mcm2–7 complexes are loaded around the origin DNA (Coster et al., 2014; Kang et al., 2014). Helicase loading requires opening and closing of the toroidal Mcm2–7 ring between the Mcm2 and Mcm5 subunits (Bochman and Schwacha, 2008; Costa et al., 2011; Samel et al., 2014). The product of helicase loading is a pair of tightly interacting Mcm2–7 complexes that encircle the double-stranded origin DNA in a head-to-head conformation, with staggered Mcm2/5 gates (Costa et al., 2014; Evrin et al., 2009; Remus et al., 2009; Sun et al., 2014).

Although the structure of the double-hexamer product of helicase loading is clear, important questions remain about how the helicase-loading proteins achieve this outcome. In particular, the mechanisms that load the first and second Mcm2–7 complex in opposite orientations are unclear (reviewed in Yardimci and Walter, 2014). Do the two Mcm2–7 complexes associate and load simultaneously or in an ordered fashion? Do the same or different ORC and Cdc6 proteins load each Mcm2–7 complex? To address these questions, we have developed single-molecule assays to monitor helicase loading.

Single-molecule studies are a powerful tool to address questions of stoichiometry and dynamics during DNA replication events. Studies of this type have led to important insights including the dynamics and number of DNA polymerases acting at the replication fork (reviewed in Stratmann and van Oijen, 2014). Extending these approaches to replication initiation has the potential for additional discovery. Unlike current ensemble helicase loading assays, which can only detect events that survive multiple washes, single-molecule approaches readily detect short-lived interactions during cycles of enzymatic function. Single-molecule approaches also allow stoichiometric determinations that are difficult with ensemble helicase loading assays due to DNA-to-DNA asynchrony and heterogeneity. Finally, although multi-step reactions are frequently asynchronous, post hoc synchronization of single-molecule data allows precise kinetic analysis of reaction pathways.

We have developed single-molecule assays that monitor the DNA association of eukaryotic helicase-loading proteins using colocalization single-molecule spectroscopy (CoSMoS) (Friedman et al., 2006; Hoskins et al., 2011). We show that the two Mcm2–7 hexamers are recruited and loaded in separate events that require distinct Cdc6 and Cdt1 molecules. In contrast, one ORC molecule directs loading of both Mcm2–7 complexes present in a double hexamer. Consistent with distinct mechanisms loading the two hexamers, we observe kinetic differences between events associated with loading the first and second

helicase. By combining CoSMoS with fluorescence resonance energy transfer (FRET), we demonstrate that formation of the Mcm2–7 double-hexamer interface precedes dissociation of Cdc6 and Cdt1, suggesting interactions with the first Mcm2–7, rather than ORC, drive recruitment of the second helicase. Our observations reveal both the complex protein coordination required to assemble Mcm2–7 double hexamers and the mechanisms ensuring the two Mcm2–7 molecules are loaded in the opposite orientations required for bidirectional replication initiation.

RESULTS

A Single-Molecule Assay for Helicase Loading

To develop a single-molecule assay for eukaryotic helicase loading, we used CoSMoS to monitor the origin-DNA association of the proteins required for this process (ORC, Cdc6, Cdt1, Mcm2–7). First, we immobilized origin-containing DNA by coupling it to microscope slides. We determined the location of surface-attached DNA on the slide using a DNA-coupled fluorophore (Figure 1A). We monitored associations of one or two proteins (labeled with distinguishable fluorophores) with origin DNA using colocalization of the protein- and DNA-associated fluorophores (Figure S1A). Fluorescent labeling of ORC, Cdc6, Cdt1, and Mcm2–7 was accomplished using a SNAP-tag or sortase-mediated coupling of fluorescent peptides (Gendreizig et al., 2003; Popp et al., 2007). In each case, the fluorescent tags did not interfere with protein function in ensemble helicase-loading reactions (Figure S1B). After imaging the locations of slide-coupled DNA molecules, purified ORC, Cdc6, and Cdt1/Mcm2–7 were added (one or two of which were fluorescently labeled), and the location of each DNA molecule was continuously monitored for labeled protein colocalization in 1-s intervals for 20 min.

Multiple observations indicated that Mcm2–7-DNA colocalizations represented events of helicase loading (Table S1; Movies S1, S2, and S3). First, colocalizations of Mcm2–7 with the DNA were dramatically reduced in the absence of ORC or Cdc6, proteins required for helicase loading (Yardimci and Walter, 2014). Second, stable association (>30 s) of Mcm2–7 was dependent on the presence of the ORC DNA binding site (the ARS-consensus sequence, ACS). Third, ORC, Cdc6, origin DNA, and ATP hydrolysis were each required to form Mcm2–7 molecules that were resistant to a high-salt wash (Table S1), a biochemical test for loaded helicases encircling double-stranded DNA (dsDNA) independently of helicase-loading proteins (Donovan et al., 1997; Randell et al., 2006).

Mcm2–7 Association and Loading Occurs in a One-at-a-Time Manner

Our initial studies monitored Mcm2–7 association with origin DNA. We performed CoSMoS helicase-loading experiments using Mcm2–7 containing SNAP-tagged Mcm4 labeled with 549 fluorophore (Mcm2–7^{4SNAP549}; Figure 1) and unlabeled ORC, Cdc6, and Cdt1. Over the course of 20 min, we observed both single- and double-stepwise increases in Mcm2–7-associated fluorescence intensity at origin DNAs (Figures 1B and S1C). Mcm2–7 dwell-time distributions were multi-exponential with many short-lived (<30 s) and fewer longer-lived (>30 s) relative increases in fluorescent intensity, suggesting at least two distinct types of Mcm2–7 association with the DNA (Figure 1C).

There are two possible explanations for the multiple stepwise increases in DNA-colocalized Mcm2–7-coupled fluorescence. The simplest interpretation of this data is that Mcm2–7 hexamers associate with origin DNA in a one-at-a-time manner, with multiple hexamers accumulating over time. Alternatively, it was possible that each increase in fluorescence was due to the simultaneous association of a Mcm2–7 multimer (e.g., a pre-formed dimer of two Mcm2–7 hexamers). To distinguish between these possibilities, we used photobleaching to count the number of DNA-associated Mcm2–7 hexamers. To this end, we first observed Mcm2–7^{4SNAP549} associations with DNA and then washed the surface-tethered DNA molecules with reaction buffer, removing unbound proteins. Then, to promote photobleaching, we increased laser excitation power and removed oxygen scavengers. Comparison of the number of Mcm2–7^{4SNAP549} photobleaching steps after the wash with the number of association steps that accumulated before the wash showed no single-step increase in fluorescence before the wash resulted in a two-step photobleaching afterward (Figure 1D, top). We confirmed that loss of fluorescence was due to photobleaching and not dissociation of Mcm2–7 by observing previously non-illuminated microscope fields of view. These data eliminate models in which multiple Mcm2–7 complexes are recruited simultaneously. We conclude that Mcm2–7 association occurs in a one-at-a-time manner.

We next asked whether loading of salt-resistant Mcm2–7 hexamers around origin DNA occurred sequentially or simultaneously. We used the same photobleaching assay (described above) except a high-salt wash was used to remove any incompletely loaded Mcm2–7 complexes prior to photobleaching. If loading of both Mcm2–7 hexamers occurs simultaneously, we should observe only even numbers of high-salt-resistant hexamers. In contrast, if loading occurs sequentially, we should observe even and odd numbers of high-salt-resistant hexamers. At low protein concentrations, we observed both one- and two-step photobleaching events (Figures 1D, bottom, and 1E). Roughly half (79/160) of all single Mcm2–7-associated fluorophores that colocalized with origin DNA before the high-salt wash were high-salt resistant, and 67% (40/60) of the double-Mcm2–7-associated fluorophores were high-salt resistant. When we increased protein concentrations, we also observed DNA molecules with three and four origin-dependent, high-salt-resistant Mcm2–7 complexes (Figure S1D), indicating that more than one double-hexamer loading event occurred at a single origin.

We considered the possibility that the apparent colocalization of odd numbers of loaded Mcm2–7 complexes was due to incomplete fluorescent labeling of Mcm2–7. For example, a single salt-resistant Mcm2–7-associated fluorophore could be the result of loading two Mcm2–7 complexes, only one of which is fluorescently labeled. To address this possibility, we purified Mcm2–7 complexes that were labeled on two subunits with different fluorophores (Mcm2–7$^{4SNAP549/7SORT649}$). Because the SNAP-tag and sortase labeling approaches are independent of each other, we could use single-molecule imaging to determine

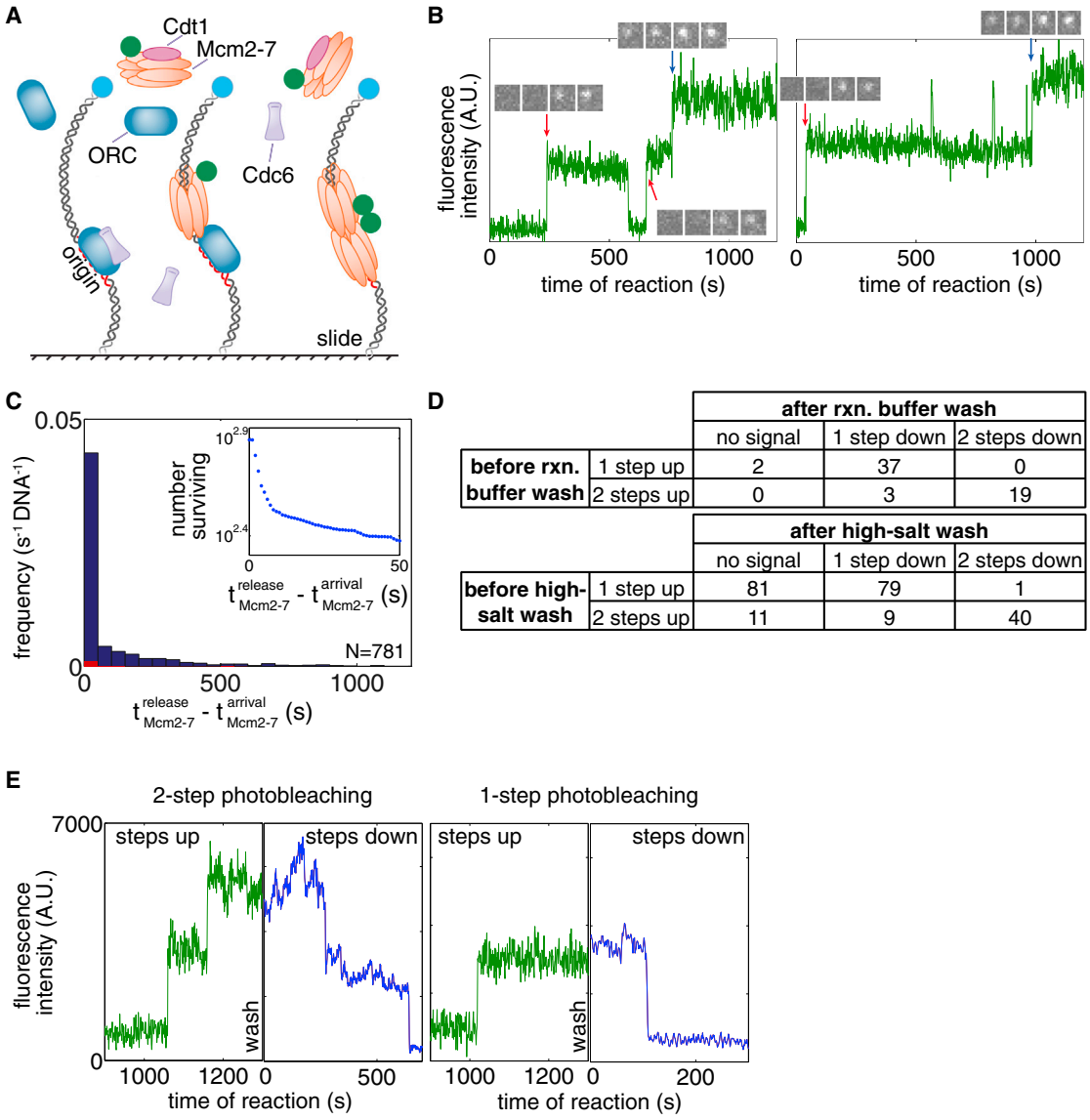

		after rxn. buffer wash		
		no signal	1 step down	2 steps down
before rxn. buffer wash	1 step up	2	37	0
	2 steps up	0	3	19

		after high-salt wash		
		no signal	1 step down	2 steps down
before high-salt wash	1 step up	81	79	1
	2 steps up	11	9	40

Figure 1. Mcm2–7 Hexamers Associate with and Are Loaded on DNA in a One-at-a-Time Manner

(A) Schematic for the single-molecule helicase-loading assay. Alexa-Fluor-488-labeled (blue circle) 1.3 kb origin DNAs were coupled to microscope slides. Purified ORC, Cdc6, and Cdt1/Mcm2–7 (at least one fluorescently labeled, Mcm2–7 in this illustration) were incubated with slide-coupled DNA, and colocalization of the fluorescently labeled protein with the DNA was monitored.

(B) Mcm2–7 complexes sequentially associate with origin DNA. Plots display the Mcm2–7^{4SNAP549} fluorescence intensity recorded at two representative DNA molecules. Insets show fluorescence images (4 × 1 s) taken during the sequential association of first (red arrow) and second (blue arrow) Mcm2–7.

(C) Mcm2–7 dwell times on DNA have a multiexponential distribution. Mcm2–7 dwell times were plotted as a histogram. Combined data from first and second Mcm2–7 associations are included; vertical axis represents the number of dwells of the specified duration per second per DNA molecule. Red bars are results from a separate experiment using mutant origin DNA. Inset shows the distribution of Mcm2–7 dwell times on DNA molecules as a semilogarithmic cumulative survival plot; only a portion of the entire plot is shown to emphasize that the distribution has at least two exponential components.

(D) Mcm2–7 associates with DNA one at a time. The number of associations present at standard protein concentrations before a reaction buffer (top) or high-salt buffer (0.5 M NaCl; bottom) wash is compared to the number of fluorophores that are detected by photobleaching immediately after the wash.

(E) Two representative traces before and after a high-salt wash and photobleaching. Reactions were washed twice with a high-salt buffer and imaged at higher laser power in the absence of an oxygen scavenging system until all fluorophores were photobleached. Traces of Mcm2–7^{4SNAP549} associations during the reaction (green) are plotted adjacent to photobleaching steps after a high-salt wash (blue).

the efficiency of each labeling protocol (79% for SNAP and 77% for sortase). This labeling protocol also increased the proportion of Mcm2–7 complexes that have at least one coupled fluorophore to 95%. Using the measured labeling efficiencies, we determined the number of high-salt-resistant Mcm2–7 complexes with no more than one of each fluorophore that would

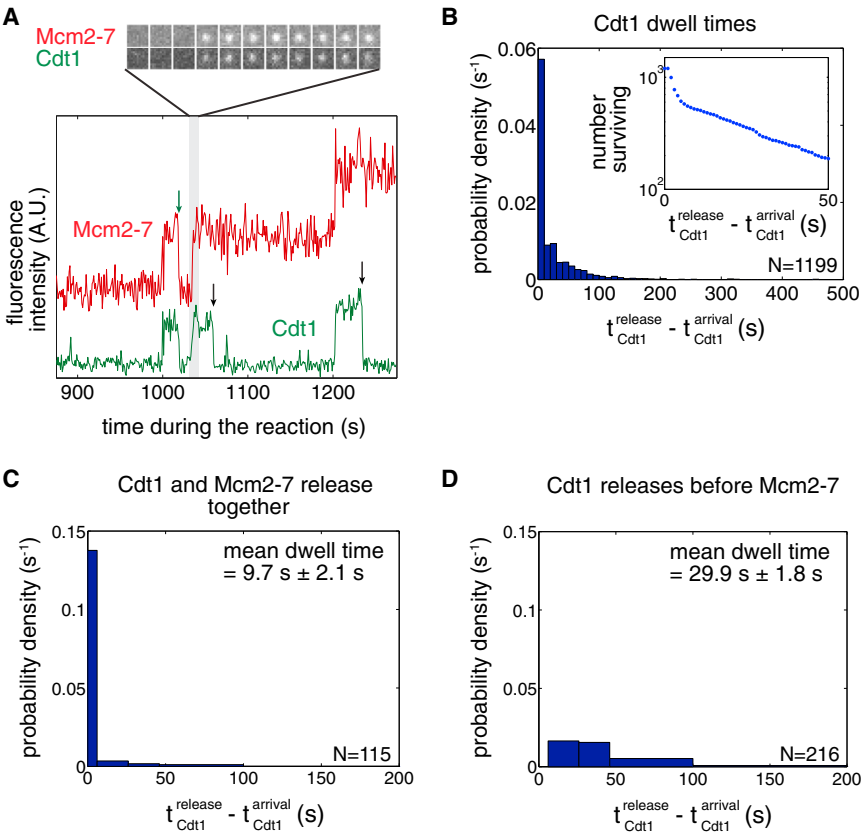

Figure 2. Distinct Cdt1 Molecules Load the First and the Second Mcm2–7 Hexamer

(A) Cdt1 molecules arrive with Mcm2–7 but release quickly after the complex arrives. A representative two-color recording of Mcm2–7^{4SNAPJF646} and Cdt1^{SORT549} fluorescence at an origin-DNA location is shown. The baseline of the red plot (Mcm2–7) is shifted up relative to the green plot (Cdt1) throughout when two-color recordings are displayed together. The sequence of single-frame images of the Cdt1- and Mcm2–7-fluorescent spots illustrates the concurrent arrival of Cdt1 and Mcm2–7. Cdt1 release occurs either with (green arrow) or without (black arrows) concurrent Mcm2–7 release.

(B) Cdt1 dwell times on DNA have a multi-exponential distribution. Cdt1 dwell times were plotted as a histogram. Inset shows semi-logarithmic cumulative survival plot as in Figure 1C.

(C and D) There are two types of Cdt1 release events. (C) Histogram shows the duration of Cdt1 origin-DNA associations when Cdt1 releases with Mcm2–7. The mean dwell time ±SEM is reported. (D) Histogram shows the duration of Cdt1 origin-DNA associations when Cdt1 releases before Mcm2–7. The mean dwell time ±SEM is reported.

be expected if only double hexamers were loaded (Figure S1E, model II). Assays with Mcm2–7$^{4SNAP549/7SORT649}$ yielded single, salt-resistant fluorophores in a proportion that is inconsistent with this model. Instead, our data are consistent with a model where both single and double hexamers are loaded (in a 52:48 ratio based on our data; Figure S1E, model I). We conclude that Mcm2–7 complexes are both recruited and loaded onto origin DNA in a sequential manner.

Distinct Cdc6 and Cdt1 Molecules Load the First and Second Mcm2–7

We investigated the number of Cdt1 and Cdc6 molecules required for helicase loading and their relative times of DNA association. Both proteins are essential for loading but show little or no association with DNA in bulk assays (Coster et al., 2014; Kang et al., 2014), suggesting that their protein and/or DNA associations during helicase loading are transient. To detect these associations, we simultaneously monitored the binding of two different protein pairs labeled with distinguishable fluorophores: either Cdt1^{SORT549} with Mcm2–7^{4SNAPJF646} or Cdc6^{SORT549} with Mcm2–7^{4SNAPJF646}. The associations of both fluorophores with origin DNA were monitored simultaneously, revealing relative times of arrival and departure for the two molecules in each pair.

Consistent with being recruited to origins as a complex, we typically observed that Cdt1 and Mcm2–7 associated with origin DNA simultaneously (Figure 2A; Figures S2A–S2C). Uncommon instances where Cdt1 or Mcm2–7 are seen associating separately (Cdt1 alone: 11.4%, Mcm2–7 alone: 18.6%) are likely caused by incomplete dye labeling of the other protein because the frequencies of these events are similar to the fractions of unlabeled Mcm2–7 or Cdt1 (14% and 20%, respectively). Like Mcm2–7, Cdt1 dwell times followed a multi-exponential distribution, indicating the presence of at least two types of Cdt1-containing complexes on the DNA (Figure 2B). Consistent with this interpretation, we identified two classes of Mcm2–7/Cdt1 dwell-time and departure behaviors. In many instances, Cdt1 and Mcm2–7 were released simultaneously (i.e., within 1 s, see Figures S2B and S2C). This release pattern occurs whether or not the DNA molecule already had an associated Mcm2–7. These associations were typically short lived (Figure 2C) and represent non-productive binding events. Interestingly, these events were less frequent if the Mcm2–7/Cdt1 was the second (29%) rather than the first (53%) to arrive at the DNA. In the remaining cases, Cdt1 was typically longer lived (Figure 2D) and was released from origin DNA by itself, leaving behind an associated Mcm2–7. Clearly, only instances when Cdt1 is released independently of Mcm2–7 can be on the pathway for double-hexamer formation. Because Cdt1-associated fluorophore photobleaching was much slower than Cdt1 dissociation (Figure S2D; Table S2), nearly all loss of fluorescent colocalization was due to dissociations, not photobleaching.

Like Cdt1, Cdc6 association with the DNA is dynamic with distinct molecules acting during loading of the first and second Mcm2–7 (Figure 3A; Figure S3A). Simultaneous analysis of Mcm2–7 and Cdc6 DNA association showed short Cdc6-DNA associations (mean lifetime 27.8 ± 1.5 s; Figure S3B), a subset of which directed Mcm2–7 recruitment (35.8%, n = 514;

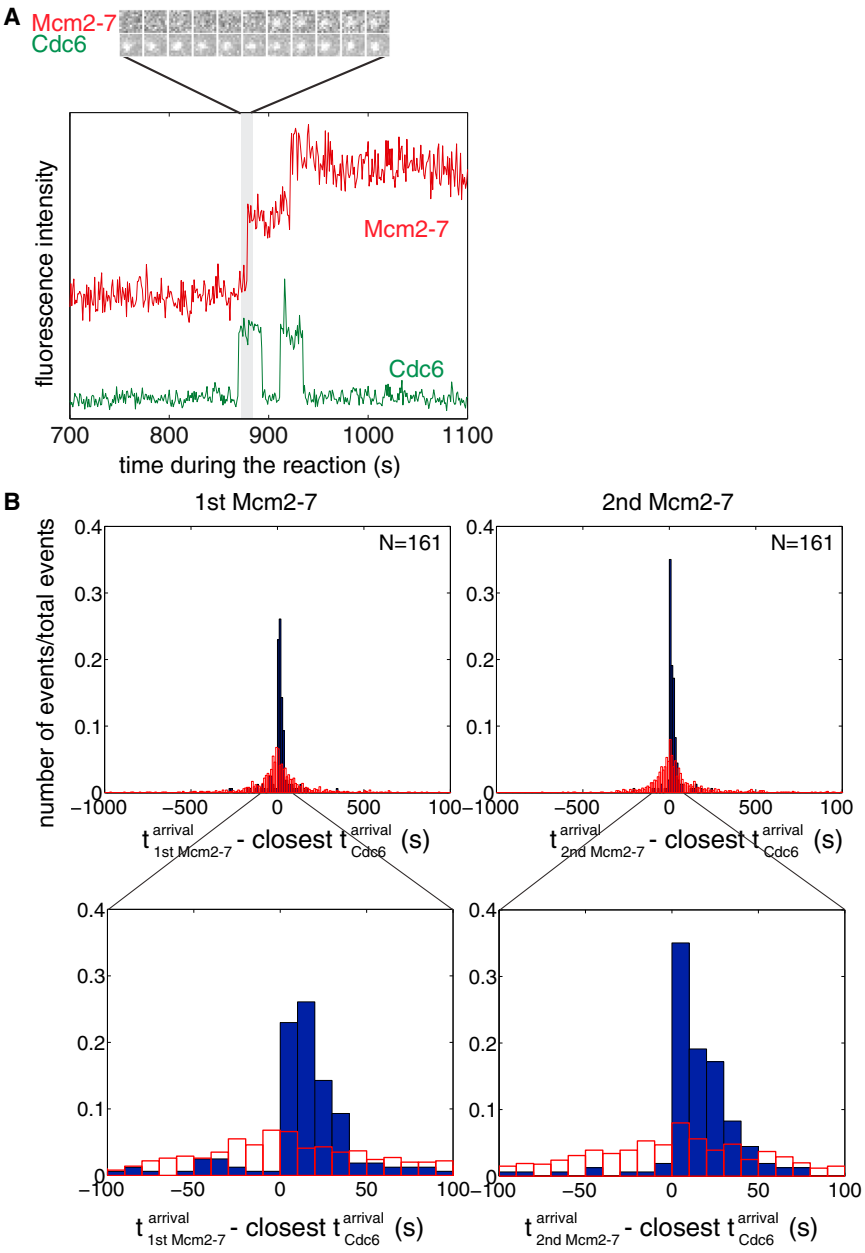

Figure 3. Distinct Cdc6 Molecules Recruit and Load the First and the Second Mcm2–7 Hexamer

(A) Distinct Cdc6 molecules anticipate each Mcm2–7 association. A representative fluorescence intensity record for Mcm2–7^{4SNAPJF646} and Cdc6^{SORT549} at origin DNA. Images of the Cdc6- and Mcm2–7-associated fluorescent spots show Cdc6 binds before the arrival of the first Mcm2–7 complex.

(B) Cdc6 association anticipates binding of the first and second Mcm2–7. Full histogram (top) and expanded view (bottom) of Mcm2–7 arrival time minus the closest Cdc6 arrival time on the same DNA molecule (blue bars). Data are separated into Mcm2–7 complexes arriving at the DNA first (left) or second (right). In >85% of the observations the difference was greater than zero, indicating that Cdc6 arrived before Mcm2–7; in the remaining <15%, Mcm2–7 arrived before Cdc6 (likely due to an unlabeled Cdc6 molecule). Red bars show a control analysis in which each Mcm2–7 arrival time was paired with the closest Cdc6 arrival time on a different, randomly selected DNA molecule. The randomized control does not show the prominent peak at differences between 0 and +50 s indicating the sequential association of Cdc6 and Mcm2–7 was not coincidental.

Figures 3A and S3A). Cdc6 consistently anticipated Mcm2–7 arrival at the DNA (>85%; Figures 3A and S3A). The remaining cases likely reflected the action of unlabeled Cdc6. We observed distinct Cdc6 proteins direct recruitment of the first and second Mcm2–7 with a similar rate constant (Figure S3C). The high frequency of Cdc6 DNA associations led us to test and confirm that sequential binding of Cdc6 and Mcm2–7 was not coincidental for either Mcm2–7 loading event (Figure 3B).

Release of Cdc6 and Cdt1 Is Sequential during Helicase Loading

We next asked whether helicase loading led to a defined order of Cdc6 and Cdt1 release. We took two approaches to address this question: (1) we performed experiments in which Cdc6 and Cdt1 were labeled with different fluorophores, and (2) we compared the times of Cdc6 and Cdt1 release relative to the time of the corresponding Mcm2–7 association in the previously described double-labeled experiments (Mcm2–7^{4SNAPJF646} with either Cdt1^{SORT549} or Cdc6^{SORT549}).

When Cdc6 and Cdt1 were labeled in the same experiment, we consistently saw Cdc6 associating with and releasing from origin DNA before Cdt1 (Figure 4A; Figure S4A). Because only non-productive Cdt1-DNA interactions had dwell times less than 6 s (see Figure 2C), we excluded these molecules from our analysis. Cdc6^{SORT649} is released before Cdt1^{SORT549} in >95% of cases when Cdt1 and Cdc6 were co-localized on a DNA (Figure 4B). When the fluorophores coupled to the proteins were swapped (Cdc6^{SORT549} and Cdt1^{SORT649}), >90% of observations showed Cdc6 dissociates from origin DNA before Cdt1 (Figure S4B). This lower percentage is likely due to the higher photobleaching rate of the 649 dye (Table S2). These results suggest that Cdc6 is released prior to Cdt1 during helicase loading.

Because Mcm2–7 was unlabeled in the previous experiments, we did not know which of the Cdc6-Cdt1 DNA co-localization events directed double-hexamer formation. To address whether Cdc6 is released before Cdt1 during double-hexamer formation, we analyzed the time that each Cdc6 or Cdt1 spent on the DNA

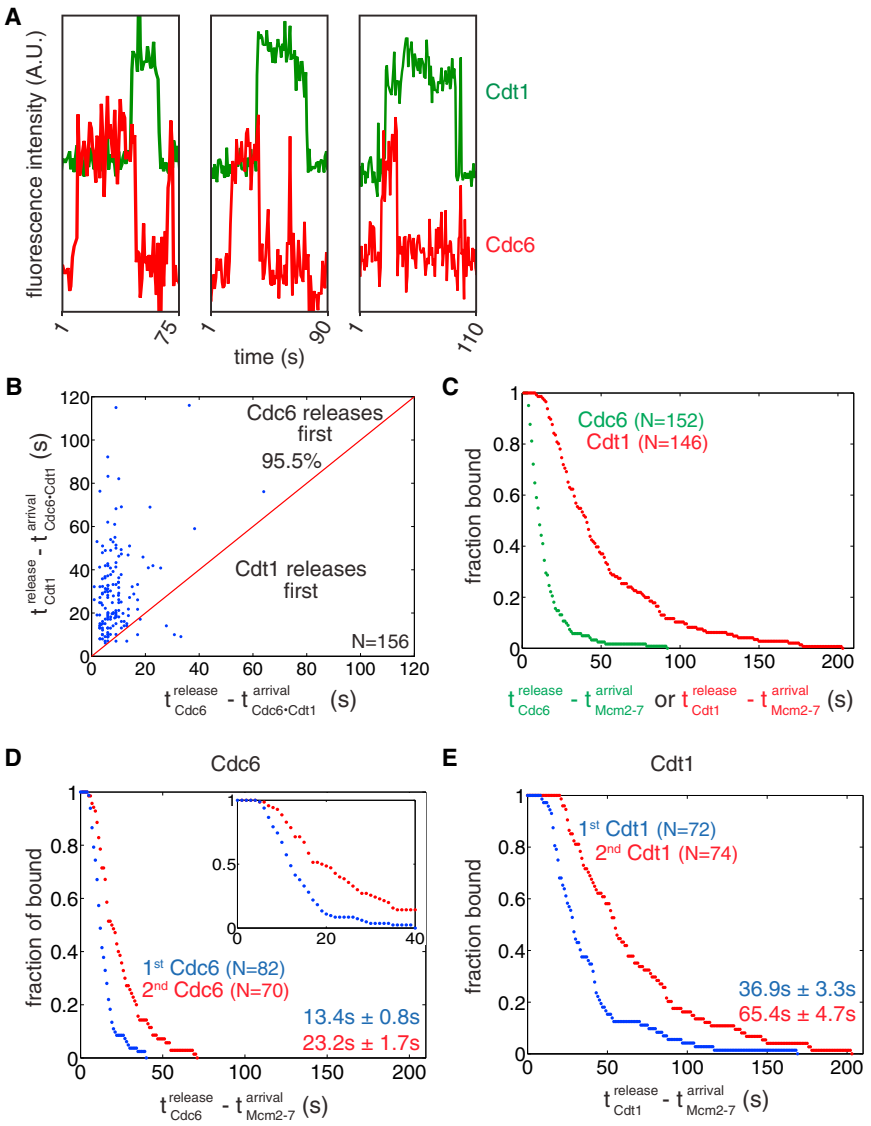

Figure 4. Cdc6 Release Occurs before Cdt1 Release

(A) Three representative fluorescence intensity records for Cdc6^{SORT649} and Cdt1^{SORT549} showing arrival and departure of Cdc6 before Cdt1.

(B) Release of Cdc6 anticipates Cdt1 release in a majority of cases. Time of Cdt1 release (y axis) is plotted against time of Cdc6 release (x axis, both times are measured from start of simultaneous presence of Cdc6 and Cdt1). The red line represents where points would fall if Cdc6 and Cdt1 released simultaneously. The fraction of measurements in which Cdc6 is released before Cdt1 is reported.

(C) Release of Cdc6 occurs before release of Cdt1 during double hexamer formation. Survival function for Cdc6^{SORT549} and Cdt1^{SORT549} dwell times after the first or second Mcm2–7 associates with origin DNA. The y axis represents the fraction of Cdc6 or Cdt1 molecules that are still associated after the time represented on the x axis.

(D and E) Cdc6 and Cdt1 release events are slower for the second versus the first Mcm2–7 loading events. (D) The time of Cdc6 release after Mcm2–7 association is plotted for the first (blue) and second (red) Mcm2–7 association as a survival plot (the fraction of Cdc6 molecules that remain DNA associated is plotted against time). Inset shows the first 40 s of the entire plot to emphasize the presence of a lag prior to DNA release. Numbers are mean release times ±SEM for the first or second Mcm2–7-associated Cdc6 molecule.

(E) Cdt1 release after the first (blue) and second Mcm2–7 association (red) as a survival plot as described for (D).

with Mcm2–7. Consistent with the Cdc6-Cdt1 double-labeling experiments, the average time between Mcm2–7 arrival and Cdc6 release is significantly shorter than the corresponding time before Cdt1 release (Figure 4C). Both the Cdc6^{SORT549} and Cdt1^{SORT549} release times are >50-fold shorter than the fluorescent dye lifetimes calculated from photobleaching rates (Table S2), verifying that these are dissociation events and not due to photobleaching. We conclude that each Mcm2–7 loading event is associated with the ordered release of Cdc6 followed by Cdt1 from the DNA.

Kinetic Evidence for Distinct Mechanisms Loading the First and Second Helicase

We reasoned that if loading of the first and second helicases occurred by different mechanisms, the time that Cdc6 and Cdt1 would spend associated with the first versus the second Mcm2–7 would differ. The resulting survival curves showed delays between arrival of Mcm2–7 and release of Cdc6 or Cdt1, suggesting that the release of both proteins involves multiple steps after Mcm2–7 recruitment. Although the order of Cdc6 and Cdt1 release remained the same, we found that the release times were significantly longer for the second Mcm2–7 loading event for both Cdc6 ($p < 0.003$; Figure 4D) and Cdt1 ($p < 0.001$; Figure 4E). These kinetic data suggest that loading of the first and second helicase occurs through distinct mechanisms.

A Single ORC Directs Formation of the Mcm2–7 Double Hexamer

There are multiple models for the stoichiometry of ORC during helicase loading (Figure S5A). One ORC molecule could direct both helicase loading events (model I). Alternatively, two ORC molecules could be present throughout the loading reaction (model II). Finally, it is possible that distinct ORC molecules direct each loading event, but both ORC molecules are only present for the second loading event (model III), or, like Cdc6 and Cdt1, each ORC is only present during loading of one Mcm2–7 (model IV). To distinguish between these models, we performed CoSMoS with simultaneous labeling of ORC and Mcm2–7.

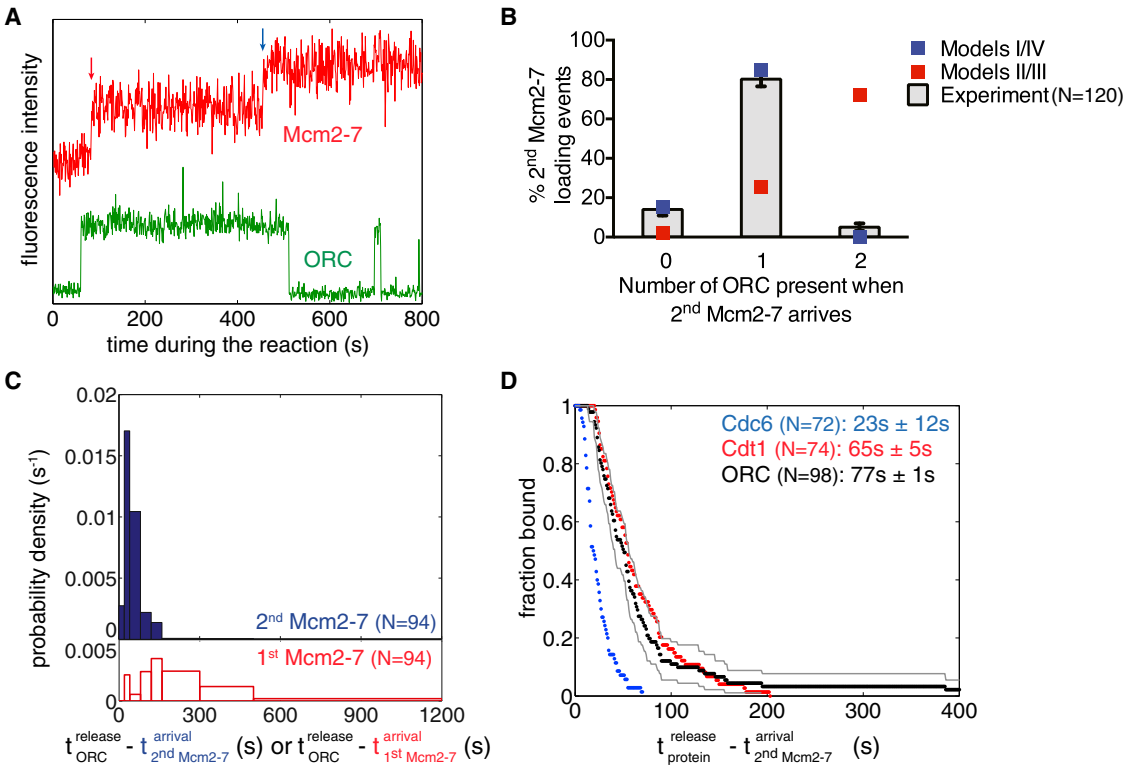

Figure 5. A Single ORC Complex Directs Recruitment and Loading of the First and Second Mcm2–7 Hexamer

(A) Representative fluorescence intensity record for ORC^{1SORT549} and Mcm2–7^{4SNAPJF646} at an origin-DNA location. Association of first and second Mcm2–7 are marked with red and blue arrows, respectively.

(B) A single ORC complex directs recruitment of two hexamers. The fraction (±SE) of DNA molecules observed to have zero, one or two ORC fluorophores bound when the second Mcm2–7 was recruited, is plotted (bars) together with the predicted number of associated fluorophores (red and blue squares) of different models (see Figure S5A).

(C) ORC is released rapidly after recruitment of the second Mcm2–7 hexamer. Histograms showing the time between the association of the second Mcm2–7 and ORC release (top) or association of the first Mcm2–7 and ORC release (bottom).

(D) Release of Cdc6^{SORT549} (blue), Cdt1^{SORT549} (red), and ORC^{1SORT549} (black) after the association of the second Mcm2–7^{4SNAPJF646} complex is plotted as a survival function. There are two ORC molecules that associate for >400 s (1,033.8 s and 709.6 s) that are not shown and disproportionately affect the mean dwell time. Gray lines represent a 95% confidence interval for the ORC data set showing that there is no significant difference between Cdt1 and ORC release time distributions. Numbers in parentheses represent the mean release times ±SEM.

Initially, we fluorescently labeled ORC on the Orc1 subunit (ORC^{1SORT549}) and observed associations with DNA in the presence of unlabeled Cdc6, Cdt1, and Mcm2–7. ORC DNA binding showed a broad distribution of dwell times (Figure S5B, left panel). Consistent with the long-lived associations reflecting ORC binding to the ACS, mutation of this element resulted in >94% of ORC DNA associations being short lived (<10 s; Figure S5B, right panel). The associations of ORC are shorter than the calculated fluorescent dye lifetimes confirming that we are observing dissociations and not photobleaching (Figure S5C; Table S2).

To identify ORC molecules involved in helicase loading, we simultaneously monitored ORC and Mcm2–7 DNA associations (Figure 5A). As expected, ORC associates with DNA and Cdt1/Mcm2–7. Unlike Cdc6 and Cdt1, we consistently observed a single increase in ORC fluorescence that remained present continuously during recruitment of the first and second Mcm2–7 complexes (Figures 5A and S5D).

Because ORC multimers have been detected (Sun et al., 2012), we addressed whether ORC complexes dimerize in solution prior to DNA binding by counting the number of photobleaching steps associated with single increases in ORC-associated fluorescence (as was described for Mcm2–7). The large majority of cases were consistent with ORC binding as a single complex (67 of 69; Figure S5E). These data confirmed that the single increases in ORC-associated fluorescence were due to single ORC molecules associating with origin DNA during loading.

Although the majority of observations involved a single ORC directing loading of two Mcm2–7 hexamers, occasionally we observed the presence of multiple DNA-bound ORC molecules at the time of a Mcm2–7 association. To address which models for ORC function during helicase loading were possible, we counted the number of DNA-associated ORC molecules (by counting stepwise increases in ORC fluorescence) during the second Mcm2–7 hexamer association (Figure 5B). Models II

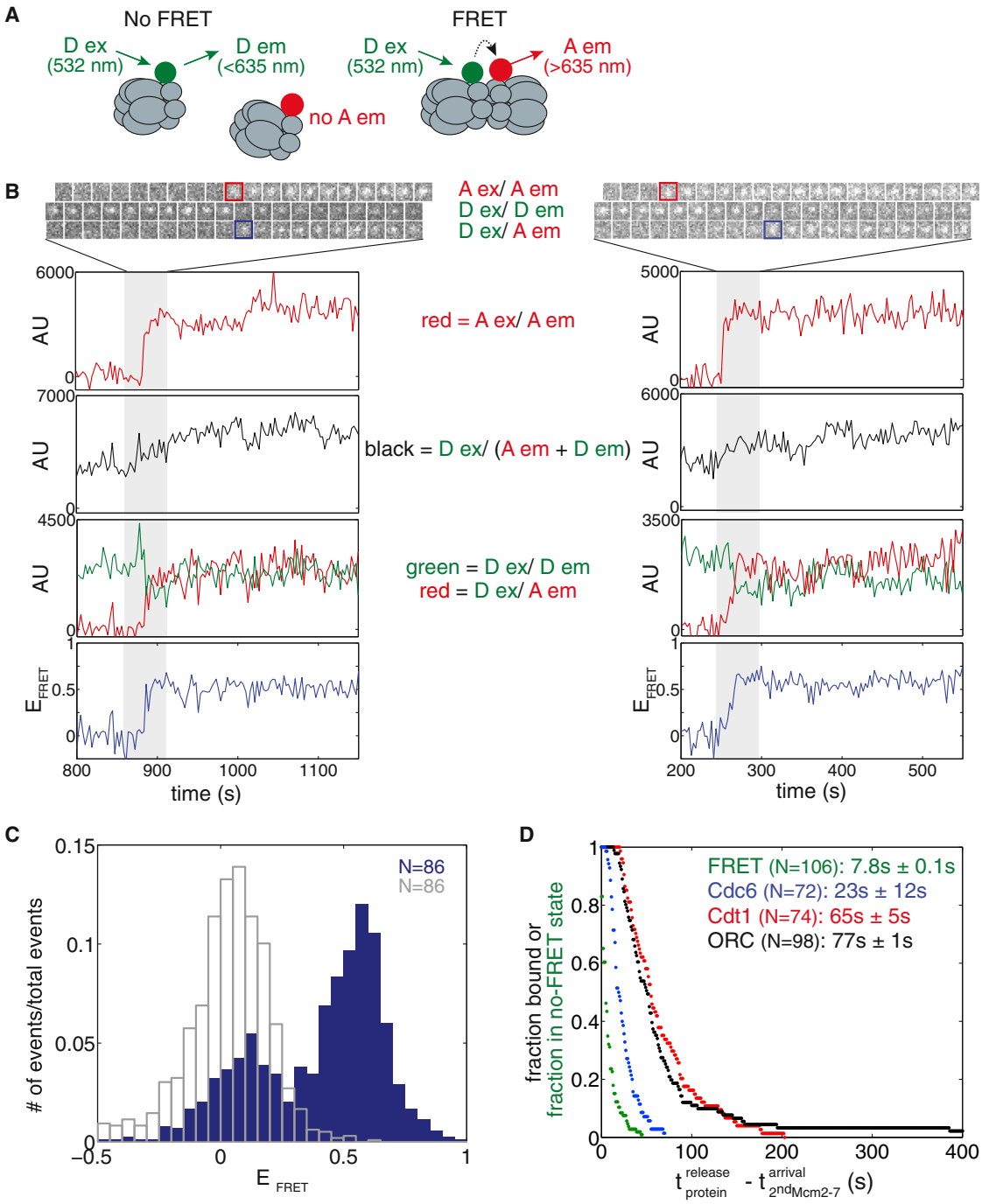

Figure 6. Double-Hexamer Formation Occurs Quickly upon Recruitment of the Second Mcm2–7 Hexamer

(A) When the two fluorophores (green circle = Dy549, red circle = Dy649) are not associated, excitation of the donor (D ex) will only yield emission from the donor (D em). However, when the two fluorophores are in close proximity, we observe acceptor emission (A em) upon D ex, and a weaker D em signal. Wavelengths represent laser excitation and emissions that were monitored.

(B) Representative fluorescence records for experiments using a mixture of Mcm2–7^{7SORT549} and Mcm2–7^{7SORT649} showing FRET upon arrival of the second Mcm2–7. Red squares highlight when Mcm2–7^{7SORT649} associates with DNA (Mcm2–7^{7SORT549} is already present), and blue squares highlight when FRET occurs. Images and records of fluorescence intensity for D ex/D em (Mcm2–7^{7SORT549}), A ex/A em (Mcm2–7^{7SORT649}), total emission (D ex / (D em + A em), and FRET (D ex/A em) are shown together with calculated E_{FRET}.

(C) Histogram of E_{FRET} is plotted for times when a single Mcm2–7^{7SORT549} and a single Mcm2–7^{7SORT649} are present (blue bars) or when only Mcm2–7^{7SORT549} is associated with the DNA (unfilled gray bars). The histogram displays the first ten consecutive E_{FRET} measurements after arrival of the second Mcm2–7 for 86 DNA

(legend continued on next page)

and III predict two ORC molecules bound to DNA when the second Mcm2–7 is recruited. In contrast to these models, we observed two ORC molecules associated during loading of the second hexamer only 5% of the time (as opposed to 70% predicted by model II or III using the measured ORC labeling efficiency; 85%; see Extended Experimental Procedures). Instead, we observe a single ORC present during association of the second helicase 80% (96/120) of the time, very close to the percentage expected if a single ORC is responsible for loading the second Mcm2–7 (85%). To distinguish between models I and IV, we asked whether the same or different ORC molecules directed the first and second helicase-loading events. Consistent with model I, 94% (n = 96) of observations showed a single ORC complex continuously present during both Mcm2–7 recruitment events. Thus, our data indicate one ORC molecule directs loading of both the first and the second Mcm2–7 hexamer (model I).

Interestingly, in most traces where two Mcm2–7 associate with the DNA, we observed dissociation of ORC from origin DNA soon after binding of the second Mcm2–7 hexamer (see Figures 5A and S5D). Plotting the times between the association of the second Mcm2–7 hexamer and ORC release (Figure 5C, blue bars), we observed only one instance where ORC released from DNA in <15 s (13.1 s), followed by a short time interval (15–90 s) during which 87% of the ORC complexes were released. The shape of this distribution suggests that, like Cdc6 and Cdt1, release of ORC is a multi-step process. In contrast, a much broader distribution was observed when ORC release was measured relative to DNA association of the first Mcm2–7 hexamer (Figure 5C, red bars), suggesting ORC release is independent of this event. To investigate the order of ORC release relative to the other helicase-loading proteins, we compared the distribution of ORC, Cdc6, and Cdt1 dwell times after binding of the second Mcm2–7 complex (Figure 5D), using data from two-color experiments with Mcm2–7^{4SNAPJF646} and 549-labeled ORC, Cdt1, or Cdc6. Photobleaching of the 549-labeled proteins was insignificant relative to their observed dwell times (Table S2). Although there is a significant difference between release of Cdc6 and ORC ($p < 0.001$), we saw no significant difference in the distributions of Cdt1 and ORC release (Figure 5D). Thus, loading of the first Mcm2–7 allows ORC retention, whereas loading of the second Mcm2–7 appears to induce the linked release of ORC and the second Cdt1.

Recruitment of a Second Mcm2–7 Results in Rapid Double-Hexamer Formation

The interactions that drive recruitment of the second Mcm2–7 remain unclear (Yardimci and Walter, 2014). To gain insight into this event, we used fluorescence resonance energy transfer (FRET)-CoSMoS (Crawford et al., 2013) to detect the proximity of the Mcm7 N-terminal domains upon double-hexamer formation (Costa et al., 2014; Sun et al., 2014). To this end, we labeled the Mcm7 subunit in separate preparations of Mcm2–7 with either 549 (Mcm2–7^{7SORT549}, donor) or 649 (Mcm2–7^{7SORT649}, acceptor) fluorophore (Figure 6A). When mixed in an equimolar ratio, the differently labeled Mcm2–7 should be in the same double hexamer ~50% of the time, and those molecules should exhibit substantial FRET efficiency (E_{FRET}) because the Mcm7 N-terminal regions are in close proximity in the double hexamer (Sun et al., 2014). We alternated between 633 and 532 nm laser excitation to monitor both arrival of each Mcm2–7 and E_{FRET}. Importantly, when Mcm2–7^{7SORT549} and Mcm2–7^{7SORT649} were sequentially recruited to the origin DNA (in either order), we observed rapid development of a high $E_{FRET} \approx 0.53$ state (Figures 6B and 6C, blue bars; Figure S6). A second peak at $E_{FRET} \approx 0.02$ was also observed in the absence of acceptor (Figure 6C, unfilled gray bars) and thus represents state(s) with no detectable FRET. Consistent with the detected FRET signal occurring as a consequence of double-hexamer formation, the high E_{FRET} state was stable for hundreds of seconds, and 95% (55/58) of the complexes that exhibited $E_{FRET} \approx 0.53$ were high-salt resistant.

To determine when double-hexamer formation occurs relative to binding of the second Mcm2–7, we compared the time of FRET formation to the time of arrival of the second Mcm2–7 (Figure 6D). We found the mean time between recruitment of the second Mcm2–7 hexamer until formation of FRET was 7.8 ± 0.1 s. This time is significantly shorter than release of Cdc6 after arrival of the second Mcm2–7 hexamer (23.2 ± 1.7 s, $p < 0.001$), indicating that formation of the N-terminal-to-N-terminal interactions anticipates, and is therefore independent of, Cdc6 and Cdt1 release (Figure 6D).

DISCUSSION

By determining precise protein/DNA stoichiometry and real-time dynamics, the single-molecule observations of helicase loading described here provide important insights into this event. Together, our findings strongly support a model in which the first and second helicase are loaded by distinct mechanisms and the second Mcm2–7 complex is recruited through interactions with the first. Accordingly, we propose a new model for helicase loading that is consistent with our current data and is described below (Figure 7).

Recruitment and Loading of Mcm2–7 Helicases Occur in a One-at-a-Time Manner

Monitoring associations in real-time reveals sequential recruitment and loading of Mcm2–7 helicases to origin DNA. One-at-a-time recruitment is consistent with an initial complex containing a single Mcm2–7 associated with the three helicase-loading proteins (Sun et al., 2013) and ensemble assays that show temporal separation of Mcm2–7 recruitment (Fernández-Cid et al., 2013). Recent structural observations indicate that the Mcm2/5

molecules (the same number of molecules and time points were used for the control). E_{FRET} data below −0.5 were excluded from the plot (3/860 signal points and 17/860 control points).

(D) Double-hexamer formation anticipates Cdc6, Cdt1, and ORC release. Survival after the association of the second Mcm2–7 complex of the no-FRET state (green) and of DNA-bound Cdc6^{SORT549} (blue), Cdt1^{SORT549} (red), and ORC^{1SORT549} (black). Mean times ±SEM until FRET increase and ORC, Cdt1, Cdc6 release are reported for comparison.

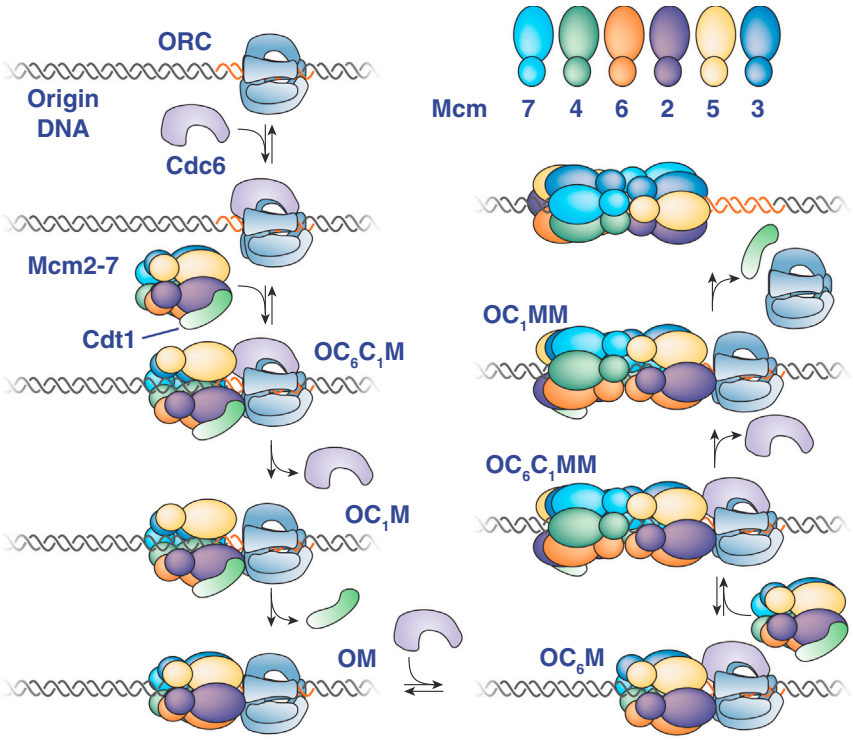

Figure 7. Proposed Model for Helicase Loading

Proteins present are indicated adjacent to each illustration (O = ORC, C_6 = Cdc6, C_1 = Cdt1, M = Mcm2–7). Reversible steps that are observed are indicated. See text for details.

gates, which must open to provide DNA access to the Mcm2–7 central channel (Samel et al., 2014), are staggered in the double hexamer (Costa et al., 2014; Sun et al., 2014). Concerted Mcm2–7 loading would require alignment of the two Mcm2/5 gates to allow simultaneous DNA entry into the central channels of both hexamers. In contrast, sequential Mcm2–7 loading can readily accommodate the formation of a staggered-gate double-hexamer structure.

Although high-salt-resistant single hexamers have been detected after artificially closing the Mcm2/5 gate (Samel et al., 2014), previous studies have not detected single loaded (high-salt resistant) Mcm2–7 complexes in unperturbed helicase-loading reactions (Evrin et al., 2009; Kang et al., 2014; Remus et al., 2009). This difference may be due to the higher protein concentrations used in these ensemble reactions. Alternatively, the high-salt-resistant single hexamers may be less stable than the double hexamers resulting in their loss during sample preparation for chromatography or EM. Indeed, a higher percentage of double hexamers showed high-salt resistance relative to single hexamers (74% versus 49%; see Figure 1D). The high-salt wash is effective in the single-molecule assay setting, however, as this treatment efficiently releases incompletely loaded Mcm2–7 formed in the absence of ATP hydrolysis (Table S1, ATPγS).

Ordered Release of Cdc6 and Cdt1 Molecules during Double-Hexamer Loading

Our studies provide insights into Cdc6 and Cdt1 function during helicase loading. Previously, robust DNA association of these proteins was only observed when helicase-loading reactions were arrested at an early ATP-dependent step. We found that the initial ORC-Cdc6-Cdt1-Mcm2–7 (OC_6C_1M) complex has two possible fates (Figure 7, left): (1) simultaneous release of Mcm2–7 and Cdt1 or (2) sequential release of Cdc6 and Cdt1 with retention of Mcm2–7. The former is most likely the reversal of the initial Mcm2–7/Cdt1 association, whereas the latter pathway leads to sequential formation of OC_1M and OM complexes and Mcm2–7 loading. Based on this distinction, we propose that release of Cdt1 independent of Mcm2–7 is coupled to successful helicase loading (illustrated as closing of the Mcm2/5 gate; Figure 7). Consistent with this hypothesis, treatments (e.g., ATPγS) or mutations (e.g., Mcm2–7 ATPase mutations, Coster et al., 2014; Kang et al., 2014) that lead to Cdt1 retention prevent helicase loading. We note that other times of ring closure (and opening) than those illustrated in the model are possible.

Electron microscopic (EM) and ensemble assays suggest the existence of helicase loading intermediates with ORC-Cdc6-Mcm2–7 (OC_6M) and ORC-Cdc6-Mcm2–7-Mcm2–7 (OC_6MM, Sun et al., 2014). Our findings suggest that the OC_6M complex is a short-lived intermediate formed prior to recruitment of the second Mcm2–7/Cdt1 complex rather than being formed by release of Cdt1 from the OC_6C_1M (Fernández-Cid et al., 2013). We do not see evidence of an OC_6MM complex during helicase loading, and there is no direct evidence that Cdc6 is present in the 2D class averages used in these studies (Sun et al., 2014). Given their relatively lower resolution, these studies could have detected either the OC_6C_1MM or OC_1MM complexes that we observe (Figure 7, right). Our previous studies found an intermediate with two Cdt1 complexes that is not detected in the current studies (Takara and Bell, 2011). During efforts to reconcile these findings, we found the Mcm2–7 protein used in the previous studies contained a non-lethal mutation in the C terminus of Mcm3 that is predicted to inhibit Cdc6 interactions (Frigola et al., 2013). We suspect that this mutant enhanced dependence on other interactions leading to the detection of two Cdt1 associations.

Loading of the First and Second Mcm2–7 Occurs by Distinct Mechanisms

In addition to answering a long-standing question about ORC function, our data indicating that one ORC molecule directs Mcm2–7 double-hexamer formation strongly suggest that

different mechanisms direct loading of the first and second Mcm2–7. EM studies suggest that during helicase loading ORC interacts with the C-terminal end of the first Mcm2–7 on adjacent DNA (Sun et al., 2014; 2013). Assuming this configuration, direct recruitment of the second Mcm2–7 complex by the same ORC would load the two Mcm2–7 molecules in a head-to-tail fashion (Figure S7, top). Even if ORC had a second binding site for Mcm2–7 on its opposite side, a similar direct interaction with Mcm2–7 could not load two Mcm2–7 complexes with adjacent N-terminal domains (Figure S7, bottom). Further evidence in favor of distinct mechanisms loading the first and second Mcm2–7 include (1) the two loading events show different Cdc6, Cdt1, and ORC release kinetics; (2) Cdt1 associated with the second loading event shows an increased propensity to release without Mcm2–7.

We considered the possibility that a second ORC binds DNA in the opposite orientation and loads the second helicase by the same mechanism as the first. Several observations argue against this model. First, because we do not consistently detect a second ORC during recruitment of the second Mcm2–7, the average dwell time for this second ORC would have to be below our detection limit (~0.5 s). This limit is >10-fold shorter than the average dwell time observed for ORC on non-origin DNA (Figure S5B). Second, in contrast to a model in which a short-lived second ORC directs loading of the second Mcm2–7, the Cdc6 protein associated with loading the second Mcm2–7 is easily detected (23.2 s average dwell time; Figure 4D). Third, even at diffusion-limited binding rates the sequential association of Cdc6 and Mcm2–7/Cdt1 with such a short-lived ORC is improbable. Finally, experiments showing that soluble ORC is not required for helicase loading if ORC is pre-loaded onto DNA (Bowers et al., 2004; Fernández-Cid et al., 2013; Duzdevich et al., 2015) are not consistent with a role for a short-lived second ORC.

Recruitment of the Second Mcm2–7

Instead of ORC and Cdc6 directly recruiting the second Mcm2–7/Cdt1 complex, our findings suggest that interactions involved in stabilizing the Mcm2–7 double hexamer mediate the recruitment of the second Mcm2–7/Cdt1. We detect these interactions prior to Cdc6 or Cdt1 release (Figure 6), suggesting that formation of double-hexamer interactions anticipates loading of the second helicase. Recent EM studies of a complex between one ORC and a head-to-head Mcm2–7 double hexamer are consistent with this hypothesis (Sun et al., 2014). Because FRET is not observed immediately upon recruitment of the second Mcm2–7, an intervening event (e.g., a Mcm2–7 conformational change or ATP hydrolysis) may be required to bring the Mcm7 N-terminal domains into close proximity. We do not know which parts of the Mcm2–7 N-terminal domains drive the proposed interactions. For simplicity, the model (Figure 7) illustrates interactions consistent with those observed in EM studies of Mcm2–7 double hexamers (Costa et al., 2014; Sun et al., 2014). One argument against a model in which Mcm2–7 N-terminal domains drive recruitment of the second Mcm2–7 is the observation that a C-terminal mutation in Mcm3 that interferes with recruitment of the first Mcm2–7 also inhibits recruitment of the second Mcm2–7 (Frigola et al., 2013). This mutant has additional defects in Mcm2–7 ATP hydrolysis, however, which could explain a loading defect for the second Mcm2–7 (Coster et al., 2014; Kang et al., 2014; Sun et al., 2014).

Because purified Mcm2–7 complexes do not show affinity for one another in solution (Evrin et al., 2009), the first Mcm2–7 must be altered to facilitate interactions with a second Mcm2–7. A likely possibility is that ORC and Cdc6 alter the conformation of the first Mcm2–7 to facilitate these interactions (shown as separation of the Mcm2/Mcm5 N-terminal regions, Sun et al., 2013). In support of a role for Cdc6, although we observe an ORC-Mcm2–7 (OM) intermediate after the first loading event, this complex is unable to recruit a second Mcm2–7 until a second Cdc6 protein associates (OC_6M).

The model for helicase loading presented here has several advantageous features. Because Cdc6 ATPase activity is required to remove incorrectly or incompletely loaded Mcm2–7 (Coster et al., 2014; Frigola et al., 2013; Kang et al., 2014), the use of different Cdc6 proteins to load the first and second Mcm2–7 would allow each event to be evaluated separately. More importantly, the use of Mcm2–7 N-terminal domain interactions to recruit the second Mcm2–7 ensures the establishment of a head-to-head double hexamer. This conformation is the first step in the establishment of bidirectional replication initiation and could be essential for initial DNA melting. Finally, the retention of ORC after the first loading event coupled with the release of ORC after the second loading event has the advantage of promoting the formation of double hexamers while inhibiting repeated loading of single hexamers.

EXPERIMENTAL PROCEDURES

Protein Purification and Labeling

Wild-type Mcm2–7/Cdt1 and ORC complexes were purified as described previously (Kang et al., 2014). Wild-type Cdc6 was purified as described in Frigola et al. (2013). We used a variety of protein fusions to fluorescently label ORC (Ubiquitin-GGG-Flag at the N terminus of Orc1), Cdc6 (GST-SUMO-GGG tag at the N terminus), and Cdt1/Mcm2–7 (Ubiquitin-GGG-Flag at the N terminus of Mcm7 or Cdt1, and/or a SNAP-tag (NEB) at the N terminus of Mcm4). The Ubiquitin (in vivo) and GST-SUMO (using Ulp1 protease) fusions were removed to reveal three N-terminal glycines required for sortase labeling. Sortase was used to couple fluorescently labeled peptide (DY549P1- or DY649P1-CHHHHHHHHHLPETGG; referred to as SORT549 and SORT649, respectively) to the N terminus of these proteins. SNAP-Surface549 (NEB, SNAP549) or SNAP-Janelia Fluor 646 (SNAPJF646; Grimm et al., 2015) was coupled to SNAP-tagged Mcm2–7 (See Extended Experimental Procedures for these purification protocols). For sortase labeling, peptide-coupled proteins were separated from uncoupled proteins using Complete-His-Tag Resin (Roche). See Extended Experimental Procedures for these purification protocols. Yeast strains and plasmids used are listed in Tables S3 and S4, respectively.

Single-Molecule Microscopy

The micro-mirror total internal reflection (TIR) microscope used for multi-wavelength single-molecule using excitation wavelengths 488, 532, and 633 nm has been previously described (Friedman and Gelles, 2012; Friedman et al., 2006). Biotinylated Alexa-Fluor-488-labeled, 1.3-kb-long DNA molecules containing an origin were coupled to the surface of a reaction chamber through streptavidin. Briefly, the chamber surface was cleaned and derivatized using a 200:1 ratio of silane-NHS-PEG and silane-NHS-PEG-biotin (see Extended Experimental Procedures). We identified DNA molecule locations by acquiring four to seven images with 488 nm excitation at the beginning of the experiment. Unless otherwise noted, helicase loading reactions contained 0.25 nM ORC, 1 nM Cdc6, and 2.5 nM Cdt1/Mcm2–7. Reaction buffer was as previously

described (Kang et al., 2014) except without any glycerol and with the addition of 2 mM dithiothreitol, 2 mg/ml bovine serum albumin (EMD Chemicals), and an oxygen scavenging system (glucose oxidase/catalase) to minimize photobleaching (Friedman et al., 2006). After addition of protein to the DNA-coupled chamber, frames of 1-s duration were acquired according to the following protocol: (1) a single-image frame visualizing the DNA positions (488 excitation), (2) 60 frames monitoring both the 549 and 649 fluorophores (simultaneous 532 and 633 excitation), and (3) a computer-controlled focus adjustment (using a 785-nm laser). This cycle was repeated roughly 20 times in the course of an experiment (~20 min). Chambers were then washed with either three chamber volumes of reaction buffer or two volumes of the same buffer with 0.5 M NaCl in place of 300 mM K-glutamate and 1 volume reaction buffer. For photobleaching, laser power(s) were increased, and one or multiple fluorophores were imaged simultaneously until no visible spots remained. Typically, photobleaching was also examined in a second field of view that was not imaged during the loading reaction.

FRET Experiments

The conditions for monitoring FRET were similar to the other experiments, with a few exceptions. Typical reactions contained 0.75 nM ORC, 3 nM Cdc6, 5 nM Cdt1/Mcm2–7^{7SORT549}, and 5 nM Cdt1/Mcm2–7^{7SORT649}. DNA was imaged before and immediately after adding the reaction to the slide but not throughout the experiment. The imaging protocol alternated between 1-s frames with the 532 laser on and 1-s frames with the 633 laser on over 20–30 min. Apparent E_{FRET} was calculated as described (Crawford et al., 2013).

SUPPLEMENTAL INFORMATION

Supplemental Information includes Extended Experimental Procedures, seven figures, three movies, and four tables and can be found with this article online at http://dx.doi.org/10.1016/j.cell.2015.03.012.

AUTHOR CONTRIBUTIONS

S.T. designed and conducted experiments with feedback from L.J.F., J.G., and S.P.B. S.T. and L.J.F. analyzed data. N.A.I. developed labeling strategies, and S.T. and N.A.I. generated proteins. S.T. and S.P.B. composed the paper with input from all authors, and S.P.B. and J.G. directed the project.

ACKNOWLEDGMENTS

We are grateful to members of the Bell laboratory for useful discussions. We thank Daniel Duzdevich and Eric C. Greene for comments on the manuscript and helpful discussions. We thank Jonathan B. Grimm and Luke D. Lavis for graciously providing the Janelia Fluors. This work was supported by NIH grants GM52339 (S.P.B.) and R01 GM81648 (J.G.) and a grant from the G. Harold and Leila Y. Mathers Foundation (J.G.). S.T. was supported in part by an NIH Pre-Doctoral Training Grant (GM007287). S.P.B. is an investigator with the Howard Hughes Medical Institute.

Received: November 13, 2014
Revised: January 26, 2015
Accepted: March 2, 2015
Published: April 16, 2015

REFERENCES

Bochman, M.L., and Schwacha, A. (2008). The Mcm2-7 complex has in vitro helicase activity. Mol. Cell *31*, 287–293.

Bowers, J.L., Randell, J.C.W., Chen, S., and Bell, S.P. (2004). ATP hydrolysis by ORC catalyzes reiterative Mcm2-7 assembly at a defined origin of replication. Mol. Cell *16*, 967–978.

Costa, A., Ilves, I., Tamberg, N., Petojevic, T., Nogales, E., Botchan, M.R., and Berger, J.M. (2011). The structural basis for MCM2-7 helicase activation by GINS and Cdc45. Nat. Struct. Mol. Biol. *18*, 471–477.

Costa, A., Renault, L., Swuec, P., Petojevic, T., Pesavento, J.J., Ilves, I., MacLellan-Gibson, K., Fleck, R.A., Botchan, M.R., and Berger, J.M. (2014). DNA binding polarity, dimerization, and ATPase ring remodeling in the CMG helicase of the eukaryotic replisome. eLife *3*, e03273.

Coster, G., Frigola, J., Beuron, F., Morris, E.P., and Diffley, J.F.X. (2014). Origin licensing requires ATP binding and hydrolysis by the MCM replicative helicase. Mol. Cell *55*, 666–677.

Crawford, D.J., Hoskins, A.A., Friedman, L.J., Gelles, J., and Moore, M.J. (2013). Single-molecule colocalization FRET evidence that spliceosome activation precedes stable approach of 5′ splice site and branch site. Proc. Natl. Acad. Sci. USA *110*, 6783–6788.

Donovan, S., Harwood, J., Drury, L.S., and Diffley, J.F.X. (1997). Cdc6p-dependent loading of Mcm proteins onto pre-replicative chromatin in budding yeast. Proc. Natl. Acad. Sci. USA *94*, 5611–5616.

Duzdevich, D., Warner, M.D., Ticau, S., Ivica, N.A., Bell, S.P., and Greene, E.C. (2015). The dynamics of eukaryotic replication initiation: Origin specificity, licensing, and firing at the single-molecule level. Mol. Cell *58*. Published online April 23, 2015. http://dx.doi.org/10.1016/j.molcel.2015.03.017.

Evrin, C., Clarke, P., Zech, J., Lurz, R., Sun, J., Uhle, S., Li, H., Stillman, B., and Speck, C. (2009). A double-hexameric MCM2-7 complex is loaded onto origin DNA during licensing of eukaryotic DNA replication. Proc. Natl. Acad. Sci. USA *106*, 20240–20245.

Fernández-Cid, A., Riera, A., Tognetti, S., Herrera, M.C., Samel, S., Evrin, C., Winkler, C., Gardenal, E., Uhle, S., and Speck, C. (2013). An ORC/Cdc6/MCM2-7 complex is formed in a multistep reaction to serve as a platform for MCM double-hexamer assembly. Mol. Cell *50*, 577–588.

Friedman, L.J., and Gelles, J. (2012). Mechanism of transcription initiation at an activator-dependent promoter defined by single-molecule observation. Cell *148*, 679–689.

Friedman, L.J., Chung, J., and Gelles, J. (2006). Viewing dynamic assembly of molecular complexes by multi-wavelength single-molecule fluorescence. Biophys. J. *91*, 1023–1031.

Frigola, J., Remus, D., Mehanna, A., and Diffley, J.F.X. (2013). ATPase-dependent quality control of DNA replication origin licensing. Nature *495*, 339–343.

Gendreizig, S., Kindermann, M., and Johnsson, K. (2003). Induced protein dimerization in vivo through covalent labeling. J. Am. Chem. Soc. *125*, 14970–14971.

Grimm, J.B., English, B.P., Chen, J., Slaughter, J.P., Zhang, Z., Revyakin, A., Patel, R., Macklin, J.J., Normanno, D., Singer, R.H., et al. (2015). A general method to improve fluorophores for live-cell and single-molecule microscopy. Nat. Methods *12*, 244–250.

Hoskins, A.A., Friedman, L.J., Gallagher, S.S., Crawford, D.J., Anderson, E.G., Wombacher, R., Ramirez, N., Cornish, V.W., Gelles, J., and Moore, M.J. (2011). Ordered and dynamic assembly of single spliceosomes. Science *331*, 1289–1295.

Kang, S., Warner, M.D., and Bell, S.P. (2014). Multiple functions for Mcm2-7 ATPase motifs during replication initiation. Mol. Cell *55*, 655–665.

Popp, M.W., Antos, J.M., Grotenbreg, G.M., Spooner, E., and Ploegh, H.L. (2007). Sortagging: a versatile method for protein labeling. Nat. Chem. Biol. *3*, 707–708.

Randell, J.C.W., Bowers, J.L., Rodríguez, H.K., and Bell, S.P. (2006). Sequential ATP hydrolysis by Cdc6 and ORC directs loading of the Mcm2-7 helicase. Mol. Cell *21*, 29–39.

Remus, D., Beuron, F., Tolun, G., Griffith, J.D., Morris, E.P., and Diffley, J.F.X. (2009). Concerted loading of Mcm2-7 double hexamers around DNA during DNA replication origin licensing. Cell *139*, 719–730.

Samel, S.A., Fernández-Cid, A., Sun, J., Riera, A., Tognetti, S., Herrera, M.C., Li, H., and Speck, C. (2014). A unique DNA entry gate serves for regulated loading of the eukaryotic replicative helicase MCM2-7 onto DNA. Genes Dev. *28*, 1653–1666.

Siddiqui, K., On, K.F., and Diffley, J.F.X. (2013). Regulating DNA replication in eukarya. Cold Spring Harb. Perspect. Biol. *5*, a012930.

Stratmann, S.A., and van Oijen, A.M. (2014). DNA replication at the single-molecule level. Chem. Soc. Rev. *43*, 1201–1220.

Sun, J., Kawakami, H., Zech, J., Speck, C., Stillman, B., and Li, H. (2012). Cdc6-induced conformational changes in ORC bound to origin DNA revealed by cryo-electron microscopy. Structure *20*, 534–544.

Sun, J., Evrin, C., Samel, S.A., Fernández-Cid, A., Riera, A., Kawakami, H., Stillman, B., Speck, C., and Li, H. (2013). Cryo-EM structure of a helicase loading intermediate containing ORC-Cdc6-Cdt1-MCM2-7 bound to DNA. Nat. Struct. Mol. Biol. *20*, 944–951.

Sun, J., Fernandez-Cid, A., Riera, A., Tognetti, S., Yuan, Z., Stillman, B., Speck, C., and Li, H. (2014). Structural and mechanistic insights into Mcm2-7 double-hexamer assembly and function. Genes Dev. *28*, 2291–2303.

Takara, T.J., and Bell, S.P. (2011). Multiple Cdt1 molecules act at each origin to load replication-competent Mcm2-7 helicases. EMBO J. *30*, 4885–4896.

Yardimci, H., and Walter, J.C. (2014). Prereplication-complex formation: a molecular double take? Nat. Struct. Mol. Biol. *21*, 20–25.

EXTENDED EXPERIMENTAL PROCEDURES

Purification and Fluorescent Labeling of Mcm2-7/Cdt1

S. cerevisiae (W303 background) strains yST147, yST161, yST166 or yST173 were grown to OD_{600} = 1.2 in 8 l of YEP supplemented with 2% glycerol (v/v) at 30°C. Addition of 2% galactose (w/v) and α-factor (100 ng/mL) induced Mcm2-7/Cdt1 expression and arrested cells at G1. After 6 hr cells were harvested and sequentially washed with 50 ml of ice-cold MilliQ water with 0.2 mM PMSF and 150 ml buffer A (50 mM HEPES-KOH [pH 7.6], 5 mM MgOAc, 1 mM ZnOAc, 2 mM ATP, 1 mM DTT, 10% glycerol, 0.02% NP-40) supplemented with 0.1 mM EDTA, 0.1 mM EGTA, 0.75 M potassium glutamate (KGlu) and 0.8 M Sorbitol. The washed pellet was resuspended in approximately 1/3 of packed cell volume of buffer A containing 0.1 mM EDTA, 0.1 mM EGTA, 0.75 M KGlu, 0.8 M Sorbitol, cOmplete Protease Inhibitor Cocktail Tablet (1 tablet per 15 ml total volume; Roche) and frozen dropwise in liquid nitrogen. Frozen cells were lysed in a SamplePrep freezermill (SPEX) and the lysate was clarified by ultracentrifugation in a Type 70 Ti rotor at 45 krpm for 90 min at 4°C. The supernatant was applied to 2 ml Anti-M2 FLAG resin (Sigma) pre-equilibrated in buffer A containing 0.1 mM EDTA, 0.1 mM EGTA and 0.75 M KGlu and incubated with rotation for 3 hr at 4°C. The resin was collected on a column and the flow-through was discarded. The resin was washed with 20 ml of buffer A with 0.3 M KGlu. Mcm2-7/Cdt1 was eluted with buffer A containing 0.3 M KGlu and 0.15 mg/mL 3xFLAG peptide. Note that for proteins with the UbSORT tag (the N-terminal methionine is replaced with the Ubiquitin followed by three glycines) the N-terminal ubiquitin is cleaved in the cells resulting in three glycines at the N terminus of the tagged Mcm2-7/Cdt1 subunit. Peak fractions containing Mcm2-7/Cdt1 were pooled, and the protein was concentrated to ~1 mg/mL using a Vivaspin 6 centrifugal concentrator (molecular weight cutoff = 100 kDa, Sartorius) and aliquoted into 0.8 ml fractions. Starting with 8 L of cells, the yield was typically 2 mg of 95% pure Sort-Mcm2-7/Cdt1, according to SDS-PAGE.

SNAP-tagged Mcm2-7/Cdt1 (Mcm2-7^{4SNAP}, Mcm2-7^{4SNAP}/Cdt1^{SORT}, Mcm2-7$^{4SNAP/7SORT}$) was labeled with SNAP-Surface549 (NEB), SNAP-Surface649 (NEB), or SNAP-JF646 by incubating with 1 nmol of dye at room temperature for 1hr. For SORT-tagged Mcm2-7/Cdt1 (Mcm2-7^{7SORT}, Mcm2-7^{4SNAP}/Cdt1^{SORT}, Mcm2-7$^{4SNAP/7SORT}$), 1 mg of Mcm2-7/Cdt1 was incubated with equimolar amount of Srt5° evolved sortase ((Chen et al., 2011), purification described below) and $CaCl_2$ was added to a final concentration of 5 mM in buffer A with 0.3 M KGlu. This was mixed with 100 nmol of peptide carrying a Sort-tag and labeled with either DY549-P1 or DY649-P1 (Dyomics), dissolved in 200 µl of buffer A with 0.3 M KGlu (sequence and fluorescent labeling of the peptide is described below). The reaction was incubated at room temperature for 15 min, and then quenched with 20 mM EDTA. The net result of the sortase reaction is coupling of the fluorescently-labeled peptide to the N terminus of the target protein with the sequence NH2-CHHHHHHHHHHLPETG followed by the remainder of the tagged protein starting at amino acid 2.

For SNAP-tagged Mcm2-7/Cdt1, after coupling the proteins to fluorophore, the reaction was applied to a Superdex 200 10/300 gel filtration column equilibrated in buffer A with 0.1 mM EDTA, 0.1 mM EGTA, and 0.3 M KGlu. Peak fractions containing Mcm2-7/Cdt1 were pooled, aliquoted and stored at −80°C.

For SORT-tagged Mcm2-7/Cdt1, after dye-coupling, the reaction was applied to a Superdex 200 10/300 gel filtration column equilibrated in buffer A with 0.1 mM EDTA, 0.1 mM EGTA, 0.3 M KGlu, and 10 mM imidazole. Peak fractions containing peptide-coupled Mcm2-7/Cdt1 were pooled and incubated with 0.5 ml of cOmplete His-Tag Purification Resin (Roche) pre-equilibrated in buffer A with 0.1 mM EDTA, 0.1 mM EGTA, 0.3 M KGlu, 10 mM imidazole, for 1 hr with rotation at 4°C. The flow-through was discarded and the resin was washed with 5 ml buffer A with 0.1 mM EDTA, 0.1 mM EGTA, 0.3 M KGlu and 10 mM imidazole. Peptide-coupled Mcm2-7/Cdt1 was eluted using buffer A with 0.1 mM EDTA, 0.1 mM EGTA, 0.3 M KGlu and 0.3 M imidazole. Peak fractions were pooled, aliquoted, and stored at −80°C.

Special note on handling of fluorescent dyes: to prevent photobleaching, all reactions containing fluorescent molecules were covered with aluminum foil and/or done in the dark room. Light sources on all machines (AKTA FPLC, HPLC) were turned off during preparative runs. Fractions containing fluorescently-labeled peptides and proteins were determined during previous analytical runs.

Determining Percent-Labeled Mcm2-7$^{4SNAP549/7SORT649}$

To determine the labeling efficiency of the SNAP-tag or sortase-labeling approaches, we purified and labeled Mcm2-7$^{4SNAP/7SORT}$ from yST173. We imaged a standard reaction containing 0.25nM ORC, 1nM Cdc6 and 2.5nM Cdt1/ Mcm2-7$^{4SNAP549/7SORT649}$ using the described protocol and monitored Mcm2-7-DNA colocalization (to ensure that we were monitoring fully assembled complexes). The DNA-associations were scored for complexes that labeled with both fluorophores or just a single fluorophore. We assumed the two labeling approaches were independent of each other and used the number of Mcm2-7 complexes that were labeled with either one fluorophore or both to determine the percent that were labeled by each approach. For example, the percentage of visible Mcm2-7^{4SNAP549} complexes that also displayed 649 fluorescence revealed the percent labeling of the SORT tag by the 649 dye.

Purification and Fluorescent Labeling of Cdc6

This protocol is based on a previously published protocol for purification of Cdc6 (Mehanna and Diffley, 2012). Plasmid harboring GST-SUMO-SORT-Cdc6 (pET23b-GST-SUMO-SORT-Cdc6) was transformed into Rosetta 2(DE3) pLysS *Escherichia coli* strain. 2 L of cells were grown in LB supplemented with 100 µg/mL ampicillin and 25 µg/mL chloramphenicol to OD_{600} = 0.6 at 37°C. Expression of GST-SUMO-SORT-Cdc6 was induced with 0.5 mM IPTG for 5 hr at 18°C. Cells were harvested by centrifugation and washed once with 50 ml of ice-cold MilliQ water containing 0.2 mM PMSF. The washed cell pellet was resuspended in 50 ml of buffer B

(50 mM K_2HPO_4/KH_2PO_4 [pH 7.5], 5 mM $MgCl_2$, 1 mM DTT, 1% Triton X-100) with 2 mM ATP, 0.15 M potassium acetate (KOAc), cOmplete Protease Inhibitor Cocktail tablet (1 tablet per 15 ml of total volume; Roche), 100 μg/mL of lysozyme and incubated for 15 min on ice. Cells were lysed by sonication and the lysate was clarified by ultracentrifugation with a 70 Ti rotor at 45 krpm for 40 min at 4°C. The clarified lysate was incubated with 2 ml bed volume of Glutathione Sepharose 4 Fast Flow (GE Healthcare) resin pre-equilibrated in buffer B with 2 mM ATP, and 0.15 M KOAc for 3 hr while rotating in the cold room. The flow-through was discarded and the resin was washed with 40 ml of buffer B with 2 mM ATP and 0.15 M KOAc. The column flow was stopped and the resin was suspended in 2 ml of buffer B with 2 mM ATP, 0.15 M KOAc and 300 μg of Ulp1 protease. The Ulp1 protease cleaves immediately after SUMO, resulting in N-terminal Sortase recognition tag (three glycines) on Cdc6. The mixture was incubated at 4°C for 10 min with occasional swirling by hand to prevent resin settling. The flow through and two 2 ml washes with buffer B with 2 mM ATP and 0.15 M KOAc were collected, pooled and the KOAc concentration was adjusted to 75 mM by adding buffer B with 2 mM ATP. The protein solution was applied to 1 ml bed volume of hydroxyapatite ceramic (BioRad, 80 μm particle size) pre-equilibrated in buffer B with 2 mM ATP and 0.15 M KOAc. The flow-through was discarded and the column was washed with 5 ml of buffer B with 2 mM ATP and 0.15 M KOAc, followed by 5 ml of buffer C (50 mM Tris-HCl [pH 7.5], 5 mM $MgCl_2$, 1 mM DTT, 15% glycerol, 1% Triton X-100), and 5 ml of buffer C with 0.15 KOAc. GGG-Cdc6 was eluted using buffer C with 0.4 M KOAc. Starting with 2 L of cells, the yield is typically 2 mg of 95% pure Cdc6, according to SDS-PAGE.

1 mg of GGG-Cdc6 was mixed with equimolar amount of Srt5° and $CaCl_2$ was added to a final concentration of 5 mM in buffer C. This was mixed with 100 nmol of peptide carrying a Sort-tag and labeled with either DY-549P1 or DY649P1 (Dyomics), dissolved in 200 μl of buffer C. Labeling was allowed to proceed for 2 min at room temperature. The reaction was terminated by the addition of 500 mM EDTA to a final concentration of 20 mM. We found that reaction times longer than 10 min result in Cdc6 aggregation. The terminated reaction was applied to a Superdex 75 10/300 gel filtration column equilibrated with buffer D (50 mM HEPES-KOH [pH 7.6], 5 mM $MgCl_2$, 1 mM DTT, 0.1 mM EDTA, 1% Triton X-100, 15% glycerol) containing 0.3 M KGlu and 10 mM imidazole. Peak fractions were pooled and incubated with 0.5 ml of cOmplete His-Tag Purification Resin (Roche) pre-equilibrated in buffer D with 0.3 M KGlu and 10 mM imidazole for 2 hr with rotation at 4°C. The flow-through was discarded and the resin was washed with 5 ml of buffer D with 0.3 M KGlu and 10 mM imidazole. Fluorescently labeled Cdc6 was eluted using buffer D with 0.3 M KGlu and 0.3 M imidazole. Peak fractions were pooled, aliquoted, and stored at −80°C.

Purification and Fluorescent Labeling of ORC

yST163 cells were grown to OD_{600} = 1.2 in 8 l of YEP supplemented with 2% glycerol (v/v). Expression of UbSORT-FLAG-ORC was induced with 2% galactose (w/v) for 3 hr at 30°C. The cells were α-factor arrested (100 ng/mL) for an additional 3.5 hr, then harvested and washed once with 50 ml ice-cold MilliQ water with 0.2 mM PMSF and once with 150 ml buffer E (50 mM HEPES-KOH [pH 7.6], 10% glycerol, 5 mM MgOAc, 1 mM ZnOAc) with 0.1 mM EDTA, 0.1 mM EGTA and 1 M Sorbitol. The washed pellet was resuspended in approximately 1/3 of packed cell volume in buffer E with 500 mM KCl, 0.1 mM EDTA, 0.1 mM EGTA, 0.01% NP-40 and cOmplete Protease Inhibitor Cocktail tablets (1 tablet per 15 ml of total volume; Roche), and frozen dropwise in liquid nitrogen. The cells were lysed with a SamplePrep Freezer/Mill (SPEX) and the lysate was clarified by ultracentrifugation in a Type 70 Ti rotor at 45 krpm for 90 min at 4°C. The supernatant was applied to 2 ml Anti-M2 FLAG resin (Sigma) pre-equilibrated in buffer E with 0.1 mM EDTA, 0.1 mM EGTA, 500 mM KCl and 0.01% NP-40 and incubated with rotation for 3 hr at 4°C. The flow-through was discarded and the resin was washed with 20 ml of buffer E with 0.1 mM EDTA, 0.1 mM EGTA, 200 mM KCl and 0.01% NP-40. SORT-ORC was eluted with buffer E with 0.1 mM EDTA, 0.1 mM EGTA, 200 mM KCl, 0.01% NP-40 and 0.15 mg/mL 3xFLAG peptide. Note that N-terminal ubiquitin is cleaved off in the cells resulting in N-terminal Sortase recognition tag on Orc1. The peak fractions were pooled and applied to 0.5 ml of SP resin (GE Healthcare) pre-equilibrated with buffer E with 0.1 mM EDTA, 0.1 mM EGTA, 200 mM KCl and 0.01% NP-40. The flow-through was discarded and the resin was washed with 5 ml of buffer E with 200 mM KCl and 0.01% NP-40. SORT-ORC was eluted using buffer E with 500 mM KCl and 0.01% NP-40. Starting with 8 L of cells, the yield is 0.5 mg of 95% pure SORT-ORC, according to SDS-PAGE.

0.5 mg of SORT-ORC was combined with equimolar amount of Srt5° and and $CaCl_2$ was added to a final concentration of 5 mM in buffer E. This was mixed with 100 nmol of peptide carrying a Sort-tag and labeled with either DY-549P1 or DY-649P1 (Dyomics), dissolved in 200 μl of buffer E. The reaction was incubated at room temperature for 15 min, and terminated by adding EDTA to 20 mM. The reaction mix was applied to a Superdex 200 10/300 gel filtration column using buffer E with 0.1 mM EDTA, 0.1 mM EGTA, 0.3 M KGlu and 10 mM imidazole. Peak fractions were pooled and incubated with 0.5 ml of cOmplete-His-Tag Purification Resin (Roche) pre-equilibrated in buffer E with 0.1 mM EDTA, 0.1 mM EGTA, 0.3 M KGlu, and 1 mM imidazole, for 1 hr with rotation at 4°C. The flow-through was discarded and the resin was washed with 5 ml of buffer E with 0.1 mM EDTA, 0.1 mM EGTA, 0.3 M KGlu and 10 mM imidazole. Fluorescently labeled ORC was eluted using buffer E with 0.1 mM EDTA, 0.1 mM EGTA, 0.3 M KGlu and 0.3 M imidazole. Peak fractions were pooled, aliquoted, and stored at −80°C.

Determining ORC Labeling Fraction

To determine what fraction of ORC molecules were fluorescently labeled, 20 μl (~4.2 μg) of labeled $ORC^{1SORT549}$ was mixed with maleimide-DY-649P1 dissolved in anhydrous DMSO, in a 1:1 molar ratio at 4°C for 10 min. The reaction was terminated with 2 mM DTT. We added 0.25 nM of the double-labeled ORC to a slide containing origin DNA and monitored ORC-DNA colocalization (to ensure that we were monitoring fully assembled complexes). The fraction of maleimide-DY-649P1-labeled ORC molecules that

also contained DY-549P1 was determined and reported as the percent labeling by the DY-549P1 (we assume that coupling of maleimide-DY-649P1 to ORC is not influenced by the presence or absence of the 549 label).

Preparation of Fluorescently Labeled Peptide for Sortase-Tagging

All peptides were synthesized using solid-phase peptide synthesis (Koch Institute) and HPLC purified before use. For N-terminal labeling of proteins (carrying the N-terminal triglycine SORT-tag) we used a peptide with the sequence: H_2N-(C)HHHHHHHHHH LPETGG-COOH. We coupled fluorophore to peptide using two approaches: (1) maleimide conjugation to the cysteine residue, or (2) NHS-ester linkage to the N-terminal amine of the peptide. The 10xHis-tag is used to purify proteins coupled to the peptide using a His-tag purification column. LPETGG is the Sortase recognition tag. Maleimide- and NHS-ester labeled peptides showed no difference in experiments and were used interchangeably. However, maleimide conjugation was more efficient (always 99% yield or greater) and was our preferred method of coupling fluorophores to the peptide.

The following protocol describes fluorescent labeling of peptides (H_2N-CH_{10}LPETGG-COOH) with maleimide-DY-549P1 or maleimide-DY-649P1 (Dyomics). The reaction buffer was prepared by dissolving 9.36 g/L of Potassium Phosphate Monobasic Anhydrous and 32.73 g/L of Sodium Phosphate Dibasic Heptahydrate in ddH_2O and if necessary the pH was adjusted to 7.0. The buffer was filtered using vacuum filtration (0.2 μm pore size) and placed in a Buchner flask with a stirring bar. The buffer was vacuum degassed for 1 hr at room temperature while stirring. After degassing, N_2 gas was bubbled through the buffer solution.

3 μmol of peptide was dissolved in 2 ml of degassed buffer. 2-3 fold molar excess of peptide relative to the maleimide dye was sufficient to drive the reaction to completion. To reduce disulfide bonds between peptides, 0.3 ml of ethanethiol (Sigma) was added to the dissolved peptide. Although poorly soluble in water (0.251 M solubility in water), this amount will reduce all disulfide bonds. Ethanethiol was removed by evaporation using a speedvac for 90 min. After removal of ethanethiol, the dissolved peptide was transferred into a fresh 5 ml tube and quickly mixed with 1 μmol of maleimide-linked fluorophore dissolved in 0.5 ml of anhydrous DMSO (Sigma). The tube was covered with aluminum foil and rotated at room temperature for 2 hr. The resulting mixture was aliquoted into ten 2 ml eppendorf tubes and lyophilized overnight.

Fluorescently-labeled peptide was separated from unlabeled peptide using HPLC. We added 0.1 M DTT to the peptide mixture before HPLC separation to improve the separation of labeled peptide from unlabeled peptide and oxidized peptide dimers. The peptide mixture was separated using a Agilent Zorbax SB-C18 column at a flow rate of 1ml/min using a gradient from 0 to 80%acetonitrile containing 0.06%TFA. Fractions containing fluorescently labeled peptide were pooled and lyophilized overnight. The labeled peptide was dissolved in 200 μl of sortase reaction buffer (50 mM HEPES-KOH pH 7.6, 0.3 M potassium glutamate, 5 mM $MgCl_2$, 10% glycerol) immediately before the labeling reaction.

Fluorescent labeling of peptide (H_2N-H_{10}LPETGG-COOH) using NHS-ester-DY-549P1 or NHS-ester-DY-649P1 used a similar protocol with the following changes. The reaction was performed in 0.1 M sodium bicarbonate buffer pH 8.3, that was filtered before use (0.2 μm pore size). 10 μmol of peptide was dissolved in 3 ml of the reaction buffer, and mixed with 1 μmol of the NHS-ester dye dissolved in 1 ml anhydrous DMSO. The reaction was incubated at room temperature for 2 hr while rotating, aliqouted into ten 2 ml eppendorf tubes and lyophilized overnight. Fluorescently labeled peptide was isolated following the same protocol as for the maleimide-labeled peptide.

Purification of Sortase A Pentamutant

Sortase A P94R/D160N/D165A/K190E/K196T (Srt5°) mutant bearing a C-terminal 6xHis-tag was evolved, purified and characterized previously (Chen et al., 2011). pET29-Srt5° was transformed into BL21(DE3) *Escherichia coli* strain, grown in 1 L of LB with 100 μg/mL kanamycin to OD_{600} = 0.6 at 37°C and the expression of Srt5° was induced with 0.4 mM IPTG for 3 hr at 30°C. Cells were pelleted by centrifugation and washed once with 50 ml of ice-cold MilliQ water. The washed pellet was resusupended in 50 ml of buffer F (50 mM Tris-HCl [pH 7.9], 300 mM NaCl, 5 mM $MgCl_2$, 10% glycerol, 0.1% NP-40) with15 mM imidazole and cOmplete Protease Inhibitor Cocktail tablet (1 tablet per 15 ml of total volume; Roche) and the cells were lysed by sonication. The lysate was cleared by ultracentrifugation in a 70 Ti rotor at 35 krpm for 30 min at 4°C and the supernatant was incubated in the cold room with 2 ml bed volume of cOmplete His-tag Purification Resin (Roche) pre-equilibrated in buffer F with 15 mM imidazole for 2 hr while rotating. The flow-through was discarded and the column was washed with 40 ml of buffer F with 10 mM imidazole. Srt5° was eluted using buffer F with 0.35 M imidazole. Peak fractions containing Srt5° were pooled and applied to pre-equilibrated Superdex 75 16/600 gel filtration column using buffer G (50 mM HEPES-KOH [pH 7.6], 200 mM KCl, 5 mM $MgCl_2$, 1 mM DTT, 10% glycerol, 0.02% NP-40). Peak fractions containing Srt5° were pooled, aliquoted, and stored at −80°C. 1 L of cells typically yields 10 mg of Srt5°, 95% pure according to SDS-PAGE.

Purification of Ulp1

A catalytically active fragment (amino acids 403-621) of Ubl-specific Protease 1 (Ulp1) that is C-terminally tagged with 6xHis was described and characterized previously (Malakhov et al., 2004). pET24d-Ulp1(403-621)-6xHis was transformed into BL21(DE3) *Escherichia coli* strain. 3 L of cells were grown to OD_{600} = 0.6 at 37°C and the expression of Ulp1 was induced with 0.5 mM IPTG for 4 hr at 30°C. Cells were pelleted by centrifugation and washed once with 50 ml of ice-cold MilliQ water. The washed pellet was resuspended in 50 ml of buffer H (50 mM Tris-HCl pH 8.0, 0.3 M NaCl, 2 mM DTT, 10% glycerol, 0.1% NP-40) with 10 mM imidazole and cOmplete Protease Inhibitor Cocktail tablet (1 tablet per 15 ml of total volume; Roche) and the cells were lysed by

sonication. The lysate was cleared by ultracentrifugation in a 70 Ti rotor at 35 krpm for 30 min at 4°C. The supernatant was incubated with 2 ml bed volume of cOmplete His-tag Purification Resin (Roche) pre-equilibrated in buffer H with 10 mM imidazole for 2 hr while rotating. The flow-through was discarded and the column was washed with 40 ml of buffer H with 10 mM imidazole. Ulp1 was eluted using buffer H with 0.35 M imidazole. Peak fractions containing Ulp1 were pooled and applied to pre-equilibrated Superdex 75 16/600 gel filtration column using buffer I (50 mM HEPES-KOH pH 7.6, 100 mM KCl, 2 mM DTT, 10% glycerol, 0.02% NP-40). Peak fractions containing Ulp1 were pooled, aliquoted, and stored at −80°C. 3 L of cells typically yielded 8 mg of Ulp1, 95% pure according to SDS-PAGE.

Slide Preparation

Microscope slides for single molecule studies were prepared using methods similar to those previously described (Gandhi et al., 2010). Specifically, we cleaned glass slides and glass coverslips using sonication in four sequential solutions (1 hr in 2% Micro-90, 1hr 0.1M KOH, 1hr 100% EtOH and 15 min deionized water in a Fisher Scientific FS30H bath sonicator). The cleaned slides and coverslips were covered with 20mg/mL mPEG-Silane-2000 and 0.1 mg/ml biotin-mPEG-Silane-3400 (Laysan Bio) (1:200 ratio) dissolved in 80% ethanol [pH 2] at 70°C for 2 hr (100 μl for the coverslip, 200 μl for the slide), resulting in the PEGylation of their surfaces. After this incubation, the slides were washed with 10 mM Tris-HCl pH 7.0, dried, and incubated two more times (20 mg/ml mPEG-silane (no biotin-mPEG) in 80% ethanol [pH 2] at 70°C for 2 hr. The slides were washed and dried between these incubations and at the end with 10 mM Tris-HCl [pH 7.0]. The PEG-treated slides were stored under N_2 gas at −80°C and used in experiments the following day. Flow chambers were constructed using high vacuum grease (Dow Corning) to separate the slides and the coverslips and to delineate flow chamber lanes. Flow chamber volumes were typically ~20 μL.

Data Analysis Procedures

Analysis of the CoSMoS data sets was similar to (Hoskins et al., 2011). Specifically, we typically followed these four steps: (1) defining the spatial relationship between the two images created at different excitation/emission wavelengths from the single field of view by the dual-view optical system (“mapping”), (2) correcting the dataset for stage drift that occurred during the experiment (“drift correction”), (3) imaging the label on origin-DNA to identify the locations of single DNA molecules on the surface, and (4) integration of fluorescence emission from small regions centered at the pre-defined locations of coupled DNA locations in each acquired image to obtain plots of fluorescence intensity versus time. These steps were carried out using custom image-processing software implemented in MATLAB [The Mathworks (Natick, MA)].

Both the dual imaging optics and chromatic aberrations result in spatial displacement between fluorescent spot images of co-localized species that are labeled with different color dyes. Accurate co-localization of the differentially labeled species therefore requires use of a mapping procedure. For each pair of colors a list of several hundred reference spot pairs were collected using a sample containing a surface-tethered oligonucleotide that was labeled with Alexa488, Cy3 and Cy5. Mapping the coordinates of a fluorescent spot to the equivalent location at a different color was performed using a transformation with fit parameters based on just the 15 nearest reference spots (Crawford et al., 2013).

Drift correction was carried out using fluorescent protein spots that had a duration of at least 50 continuous frames during the experiment. Multiple spots were chosen so as to cover the image sequence at least three times. Each spot image was fit to a Gaussian function to determine its center during every frame of the image sequence in which the spot was tracked. The changes in spot position between successive image frames were averaged for the visible tracked spots, and this described the stage drift over the experimental time course. That measured stage drift was smoothed and then used to correct the positions of all spot images recorded throughout the experiment.

Locations of the coupled-DNA molecules were determined using spot-detection image processing software (Crocker and Grier, 1996) implemented in Matlab (Blair and Dufresne, 2009). Each DNA location was manually inspected to verify that the software correctly identified the center of each spot and that no spurious signals were incorrectly identified (for example edges of the field of view or background noise) as DNA spots. Furthermore, in cases where stoichiometry of the proteins was determined, the photobleaching of the identified DNA spots was monitored to ensure that a single DNA molecule was present in each analyzed area.

Fluorescence emission from labeled complexes was integrated over a 0.37 μm^2 area centered at each drift corrected origin-DNA location, yielding for each DNA molecule a separate intensity time course for each color of fluorescent label being observed.

Fitting to Single and Double Exponential Distribution

Fitting of dwell times was performed using maximum likelihood algorithms and bootstrap methods were used to determine uncertainty estimates, similar to what has been previously described (Crawford et al., 2013; Friedman and Gelles, 2012).

FRET Data Analysis

Images containing spots that were analyzed to produce a FRET time course were first mapped and drift-corrected (see above). By alternating between their laser excitation wavelengths we monitored the co-localization of both the donor and acceptor-labeled Mcm2-7 hexamers with the origin-DNA molecule. To determine the time until formation of the high-FRET state, we noted the earliest time when both of the labeled Mcm2-7 hexamers were present and subtracted that value from the time when the > 635 nm emission FRET signal rose above background noise level (as determined by monitoring the signal in the > 635 nm field when only the 532 laser

was turned on). Spots were selected manually based on FRET signal that was above background noise and contained only one of each fluorophore.

To calculate apparent FRET efficiencies, fluorescence intensity traces were background subtracted using custom Matlab (MATHWORKS) image processing software that has been previously described (Crawford et al., 2013). FRET efficiency was calculated using $E_{FRET} = I_{Acceptor}/(I_{Acceptor} + I_{Donor})$ where $I_{Acceptor}$ and I_{Donor} are the acceptor and donor emission intensities observed during donor excitation, respectively. No gamma correction was applied because no systematic change in ($I_{Acceptor}$ + I_{Donor}) was observed upon changes in E_{FRET} (Figures 6A and S6) or upon acceptor photobleaching. For each molecule, E_{FRET} values were reported for only the first 10 frames captured (~27 s) after both fluorescently-labeled Mcm2-7 complexes associated with origin-DNA.

SUPPLEMENTAL REFERENCES

Blair, D., and Dufresne, E. (2009). MATLAB Locating and Tracking Code. http://site.physics.georgetown.edu/matlab/code.html.

Chen, I., Dorr, B.M., and Liu, D.R. (2011). A general strategy for the evolution of bond-forming enzymes using yeast display. Proc. Natl. Acad. Sci. *108*, 11399–11404.

Crocker, J.C., and Grier, D.G. (1996). Methods of digital video microscopy for colloidal studies. J. Colloid Interface Sci. *179*, 298–310.

Gandhi, M., Smith, B.A., Bovellan, M., Paavilainen, V., Daugherty-Clarke, K., Gelles, J., Lappalainen, P., and Goode, B.L. (2010). GMF is a cofilin homolog that binds Arp2/3 complex to stimulate filament debranching and inhibit actin nucleation. Curr. Biol. *20*, 861–867.

Heller, R.C., Kang, S., Lam, W.M., Chen, S., Chan, C.S., and Bell, S.P. (2011). Eukaryotic origin-dependent DNA replication in vitro reveals sequential action of DDK and S-CDK kinases. Cell *146*, 80–91.

Malakhov, M.P., Mattern, M.R., Malakhova, O.A., Drinker, M., Weeks, S.D., and Butt, T.R. (2004). SUMO fusions and SUMO-specific protease for efficient expression and purification of proteins. J. Struct. Funct. Genomics *5*, 75–86.

Mehanna, A., and Diffley, J.F.X. (2012). Pre-replicative complex assembly with purified proteins. Methods *57*, 222–226.

Tsakraklides, V., and Bell, S.P. (2010). Dynamics of pre-replicative complex assembly. J. Biol. Chem. *285*, 9437–9443.

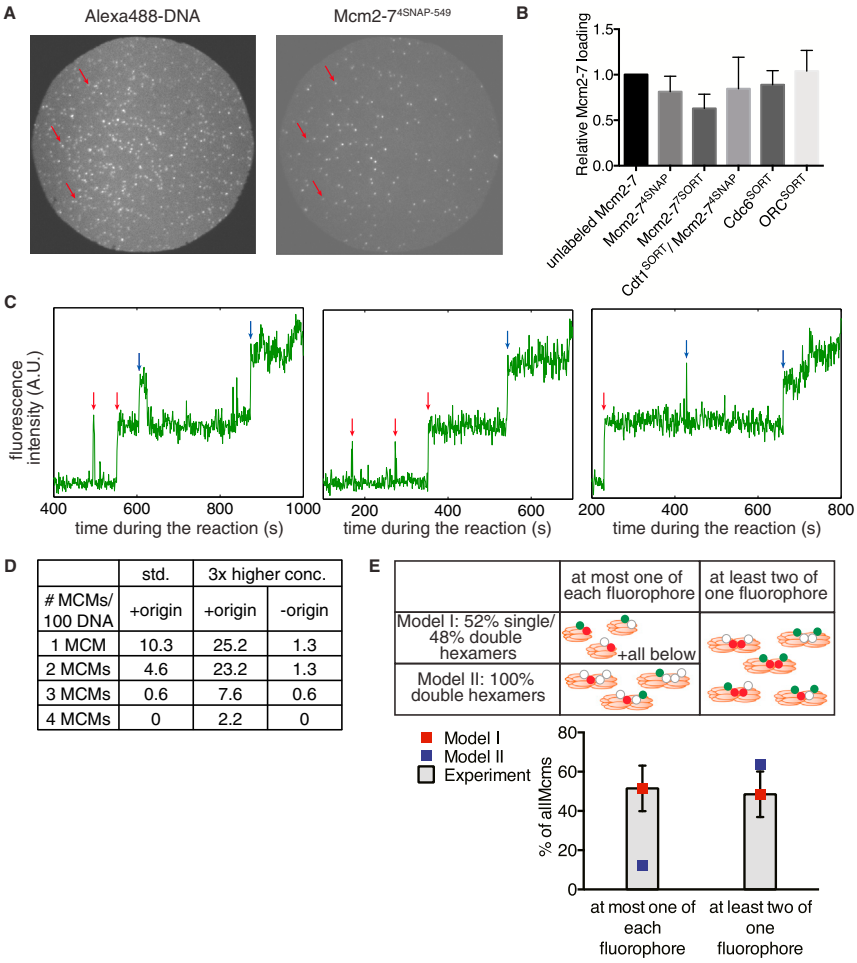

D

	std.	3x higher conc.	
# MCMs/ 100 DNA	+origin	+origin	-origin
1 MCM	10.3	25.2	1.3
2 MCMs	4.6	23.2	1.3
3 MCMs	0.6	7.6	0.6
4 MCMs	0	2.2	0

Figure S1. Mcm2-7 Hexamers Associate with and Are Loaded on DNA in a One-at-a-Time Manner, Related to Figure 1

(A) Whole microscope field of view showing AlexaFluor488-coupled DNA (left) and the Mcm2-7^{4SNAP549} fluorescent spots (right) from the same experiment at time = 600 s. The three red arrows represent DNA/Mcm2-7^{4SNAP549} colocalized pairs for which the fluorescent intensity traces are shown in S1C.

(B) Activity of fluorescently labeled proteins relative to the unlabeled proteins.

Bulk helicase-loading assays were performed using unlabeled or fluorescently-labeled Mcm2-7, Cdt1/Mcm2-7, Cdc6, and ORC. All samples were subjected to a high salt wash, separated by SDS-PAGE, stained with Krypton protein stain and quantified. Reactions were performed in duplicate and error bars indicate the standard deviation.

(C) Additional fluorescence intensity traces (from the experiment shown in S1A, see red arrows) for DNA-associated Mcm2-7^{4SNAP549} over time showing that Mcm2-7 complexes sequentially associate with origin DNA. First and second Mcm2-7 associations are marked with red and blue arrows, respectively.

(D) Mcm2-7^{4SNAP549} complexes were photobleached after a high-salt wash, and the number of high-salt resistant hexamers per 100 DNA molecules was calculated. We performed this experiment at standard (0.25nM ORC, 1nM Cdc6, 2.5nM Cdt1/Mcm2-7; N_{DNA} = 523) and three-fold higher concentrations of each of the proteins. The increased concentration experiment was performed with distinguishably-labeled wild-type (N_{DNA} = 449) and mutated ORC binding site (the ARS consensus sequence; N_{DNA} = 315) DNA molecules present in the same reaction chamber.

(E) Mcm2-7 complexes are loaded one at a time. Double-labeled Mcm2-7$^{4SNAP549/7SORT649}$ complexes were used in a standard single-molecule helicase-loading assay. This reaction was not imaged during the standard 20 min to prevent photobleaching during the reaction. Instead, after the 20 min helicase-loading reaction, the chamber was washed with high-salt buffer. Then, multiple fields of view were imaged under photobleaching conditions (Figure 1E) to determine the number of associated fluorophores for each DNA molecule. A total of 540 DNA molecules with one or more Mcm2-7-associated fluorophores were analyzed. The images in the top panels illustrate the combinations of labeled and unlabeled Mcm2-7 molecules that would be scored as having one molecule of either or both fluorophores (left column) or two copies of one or both fluorophores (right column). The rows indicate the type of labeled molecules expected for a model in which both Mcm2-7 single and double hexamers are loaded/high-salt resistant (top) or only double hexamers are loaded (bottom). White circles represent unlabeled or photobleached subunits. The observed data (gray bars; ±SE) is separated into the two categories described above and plotted with the expected numbers for each of two Models overlayed as single points on top of the observed data. The expected data for each Model was calculated using the separately measured labeling efficiencies for the two Mcm2-7 subunits: Mcm4-SNAP: 79% and Mcm7-Sortase: 77%.

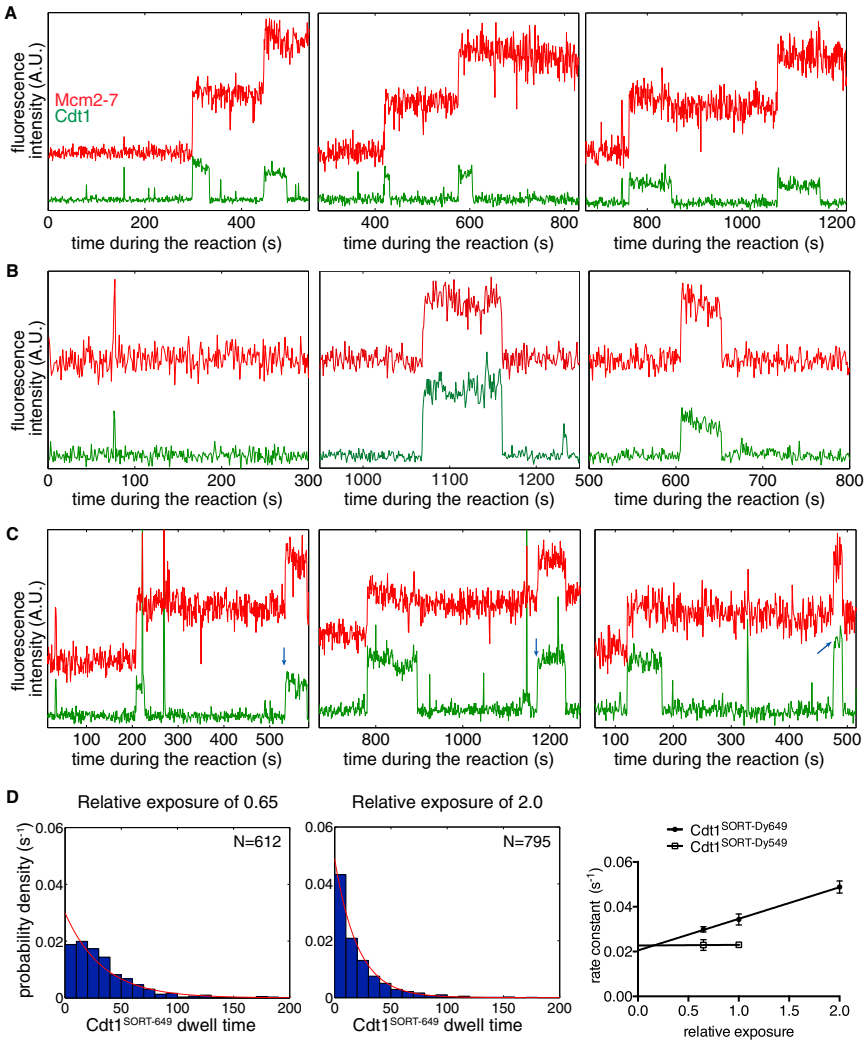

Figure S2. Distinct Cdt1 Molecules Load the First and the Second Mcm2-7 Hexamer, Related to Figure 2

(A–C) Additional fluorescence intensity records of DNA-associated Mcm2-7^{4SNAPJF646} and Cdt1^{SORT549}. Example traces show: (A) Two Mcm2-7 associations with DNA and associated Cdt1 binding and release events. (B) Mcm2-7 and Cdt1 arriving and departing simultaneously on DNA molecules without an Mcm2-7 already present. (C) Mcm2-7 and Cdt1 arriving and departing simultaneously as the second Mcm2-7 association occurring on a DNA (i.e., when an Mcm2-7 complex is already present). Second Mcm2-7/Cdt1 associations are indicated by blue arrows.

(D) Cdt1 photobleaching rate measurement. The calculated dwell times for Cdt1 were plotted for different relative laser exposures and fit either to single (649 data) or double (549 data) exponential functions. When fit to a double exponential, only the longer time constant was used to determine the photobleaching rate. Data for the experiments shown throughout the manuscript was acquired at a relative laser exposure of 1. To measure the effect of photobleaching, the relative exposure was modulated by either changing the intensity of the laser or the exposure time to the laser. We show example histograms of Cdt1^{SORT649} dwell times at a relative exposure of 0.65 (left panel; N = 612) and 2.0 (middle panel; N = 795). The red lines indicate single exponential fits. For each dye, the relative exposure (x axis) is plotted against the rate constant (y axis ±SEM). Photobleaching rate constants (slopes) from these fits are summarized in Table S2.

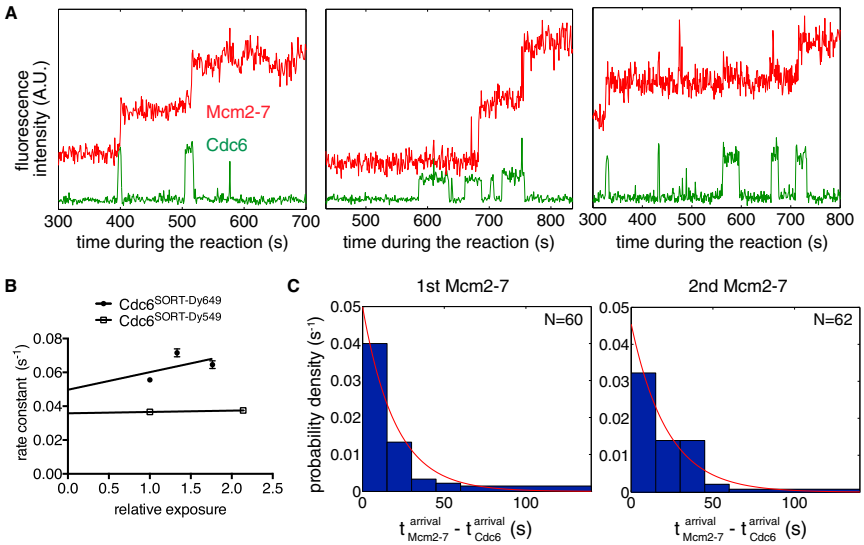

Figure S3. Distinct Cdc6 Molecules Recruit and Load the First and the Second Mcm2-7 Hexamer, Related to Figure 3

(A) Additional fluorescence intensity traces for DNA-associated Mcm2-7^{4SNAPJF646} and Cdc6^{SORT549} over time showing double hexamer associations.

(B) Measurement of Cdc6 dissociation and photobleaching rates. Cdc6 spot disappearance rate constants at different laser exposures were measured as described in Figure S2D. Dwell time distributions were fit with a single exponential model.

(C) First and second Mcm2-7 complexes associate with Cdc6-bound DNA with similar rates. Histograms showing the time of arrival of the first (left; N = 60) or second (right; N = 62) Mcm2-7 complex relative to the arrival of the associated Cdc6. Single exponential fits are plotted in red. The fits yield the following rate-constants: 0.045 s^{-1} ± 0.006 s^{-1} (for the first Mcm2-7) and 0.05 s^{-1} ± 0.01 s^{-1} (for the second Mcm2-7).

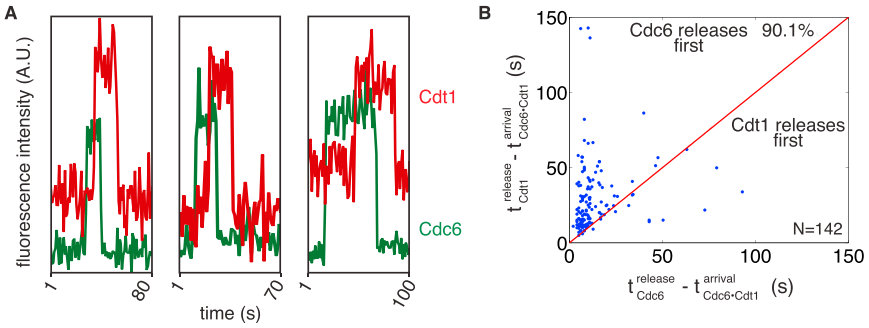

Figure S4. Cdc6 Release Occurs before Cdt1 Release, Related to Figure 4

(A) Representative fluorescence intensity trace for DNA-associated $Cdc6^{SORT549}$ and $Cdt1^{SORT649}$ over time showing arrival and departure of Cdc6 before Cdt1. (B) Release of Cdc6 anticipates Cdt1 release. Time of Cdc6 release (measured relative to the time when both Cdc6 and Cdt1 are associated, x axis) is plotted against time of Cdt1 release (also relative to when both Cdc6 and Cdt1 are present, y axis; N = 142). The red line represents where points would fall if Cdc6 and Cdt1 were released together. The percent of points falling above the red line, representing cases where Cdc6 is released before Cdt1 is reported.

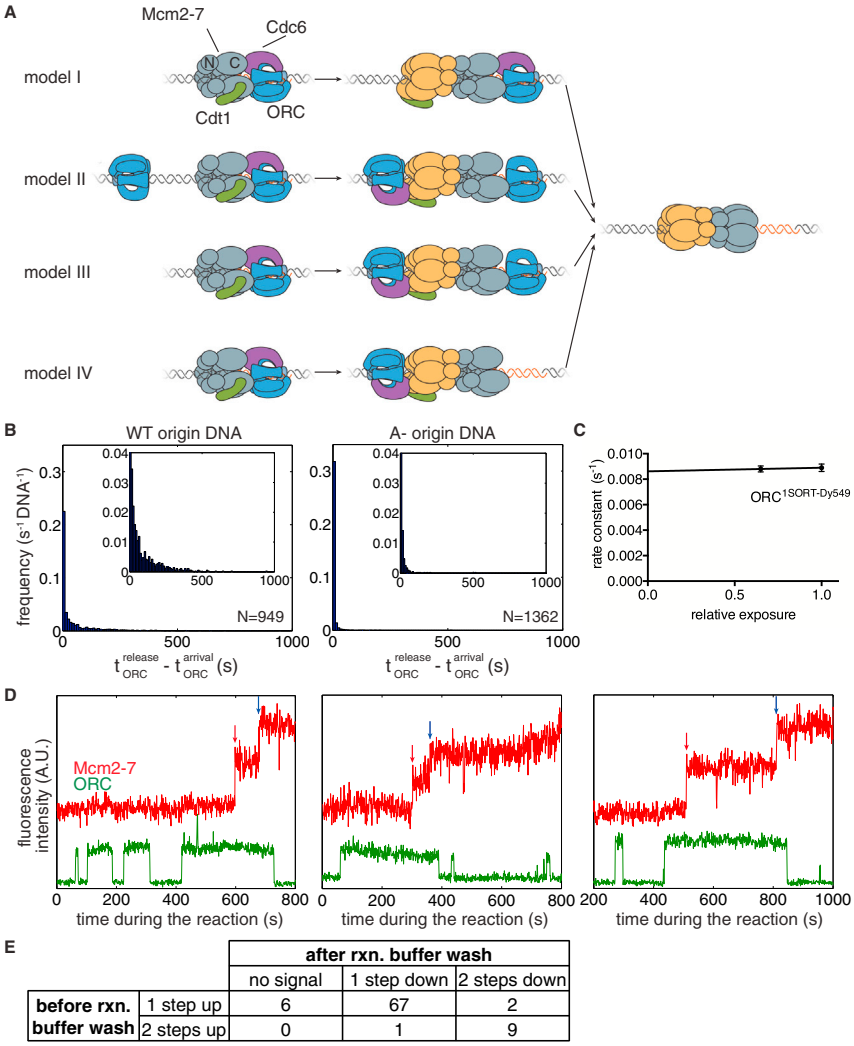

E

		after rxn. buffer wash		
		no signal	1 step down	2 steps down
before rxn. buffer wash	1 step up	6	67	2
	2 steps up	0	1	9

Figure S5. One ORC Molecule Directs Recruitment and Loading of the First and Second Mcm2-7 Hexamers, Related to Figure 5

(A) Models for ORC function during helicase loading. The initial Mcm2-7 (shown in gray) is associated with ORC/Cdc6 via its C-terminal end (Sun et al., 2013). The second Mcm2-7 is shown in yellow. See text for additional details.

(B) ORC exhibits longer dwell times in the presence of origin-containing DNA. Dwell times for ORC^{1SORT549} associations in the presence of unlabeled Cdc6, Cdt1 and Mcm2-7, are plotted as histograms for either DNA with a wild-type ACS (left panel; N = 949) or or a mutated ACS (right panel; N = 1362). Insets show expanded y-axes.

(C) Measurement of ORC photobleaching rate. Cdc6 spot disappearance rate constants at different laser exposures were measured as described in Figure S2D. Dwell time distributions were fit with a double exponential function and the long time constant was plotted against relative laser exposure.

(D) Additional representative traces of ORC^{1SORT549} and Mcm2-7^{4SNAPJF646} origin-DNA colocalizations plotted over time. Association of first and second Mcm2-7 are marked with red and blue arrows, respectively.

(E) ORC associates with DNA as a monomer. Number of ORC associations observed before a wash using reaction buffer, and the number of fluorophores that are bleached immediately after.

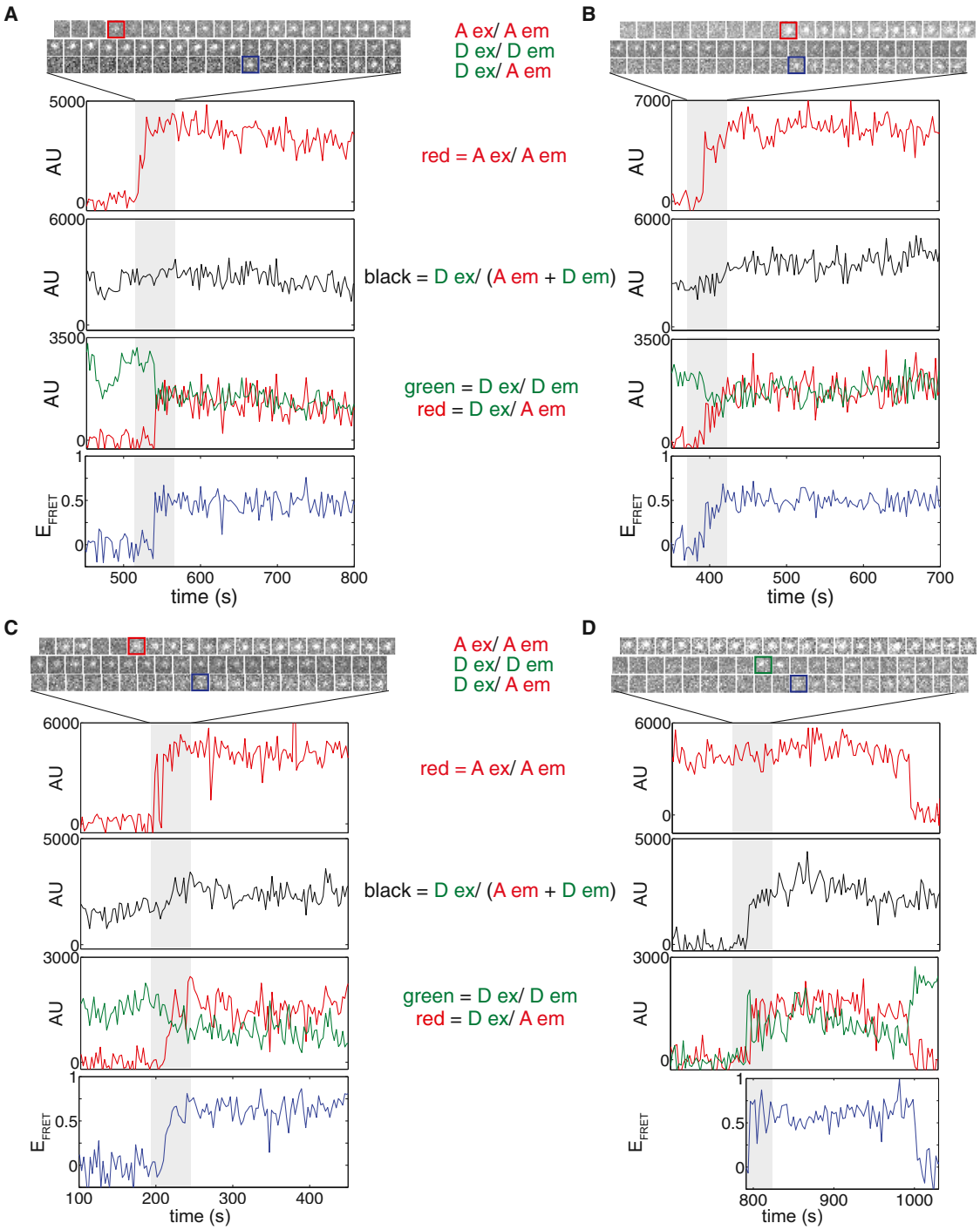

Figure S6. Double Hexamer Formation Occurs Quickly upon Recruitment of the Second Mcm2-7 Hexamer, Related to Figure 6

(A–D) Additional representative records (labeled as in Figure 6A) for experiments using a 1:1 mixture of Mcm2-7^{7SORT549} and Mcm2-7^{7SORT649} showing FRET upon arrival of the second Mcm2-7. Red squares highlight when Mcm2-7^{7SORT649} associates with DNA second (A-C), green square highlights when Mcm2-7^{7SORT549} associates with DNA second (D), and blue squares highlight when FRET occurs. In panel (D) FRET efficiency is only plotted during the time interval when Mcm2-7^{7SORT549} is present because E_{FRET} cannot be accurately measured in the absence of donor. The loss of acceptor fluorescence at ~1000 s is likely due to photobleaching of Mcm2-7^{7SORT649} and shows an associated increase in donor signal and decrease to background E_{FRET} levels.

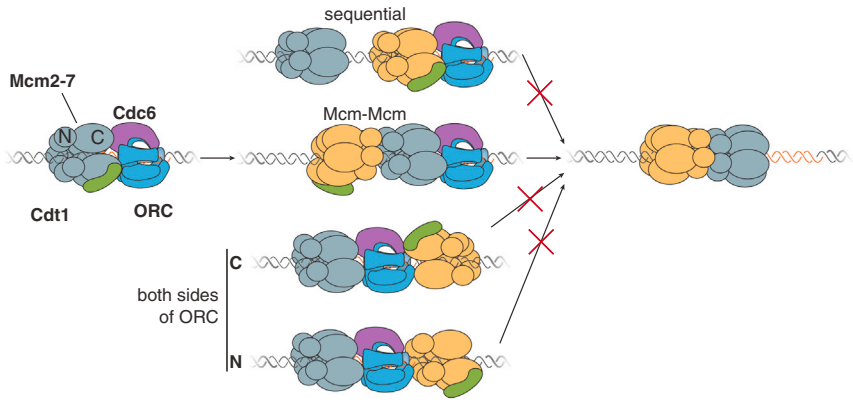

Figure S7. Proposed Model for Helicase Loading, Related to Figure 7

Three models for how a single ORC could act to load two Mcm2-7 helicases. The initial Mcm2-7 (shown in gray) is associated with ORC/Cdc6 via its C-terminal end (Sun et al., 2013). The second Mcm2-7 is shown in yellow.

(I) Sequential model. ORC recruits a second Mcm2-7 complex via the same C-terminal interactions, leading to head-to-tail double hexamers.

(II) Mcm-Mcm model. Interactions between the two N-terminal regions of the Mcm2-7 complexes recruit the second Mcm2-7 complex to yield an N-term-to-N-term double hexamer (right).

(III) Both sides of ORC model. ORC interacts with the second Mcm2-7 using its opposite face and subsequently releases. Regardless of whether recruitment of the second Mcm2-7 complex occurred via its C- or N- terminal region this model would not yield an N-term-to-N-term double hexamer (right).